Behaviour of laterally loaded monopiles

Student Name: Qianlong Chang

Student Number: 2236053

Supervisor: Dr. Hongyu Qin

Master of Civil Engineering

Civil Engineering

College of Science and Engineering

Flinders University

Contents

Figure list

Table list

ABSTRACT

With the shortage of global fossil fuel resources and human beings began to advocate low-carbon life style and environmental protection. Renewable energy has become a hot research topic, among which offshore wind power and tidal turbine are the key research objects. Offshore wind power foundation is affected by wind load and wave load all year round. Large diameter monopile is a traditional foundation structure, which can maintain the stability of offshore wind power generation structure.

This paper introduces the interaction between monopile and soil and studies the behaviour of monopile under laterally load by means of model experiment and numerical simulation. There are four contents in this study case, which are literature review, experimental analysis, numerical analysis and conclusion.

This study investigated the relationship between the horizontal displacement of monopile foundation on the sand surface and pile diameter and embedded depth through model experiment and carries out numerical simulation of large-diameter monopile foundation through RSPile software to deduce the displacement of real-size pile under laterally load.

DECLARATION

I, Qianlong Chang, certify that this thesis does not incorporate without acknowledgment any material previously submitted for a degree or diploma in any university; and that to the best of my knowledge and belief it does not contain any material previously published or written by another person except where due reference is made in the text.

Signed 

Date 08-Nov-2021

1. ACKNOWLEDGEMENTS

Thanks for my supervisor Dr. Hongyu Qin for his guidance on my study cases as well as answering the questions in my research process. Because it is the first time that I used RSPile and many details could not be mastered. With the help of Dr. Hongyu Qin, I successfully obtained the results consistent with the experimental data by this software. With his help, I saved a lot of time and used it for more comparative experiments, which made the experimental results more accurate. In addition, thanks for my friend Chao Yinghung. In my experiment, he also provided great help in the process of experimental data analysis and numerical simulation.

2. EXECUTIVE SUMMARY

Pile foundation is widely used in the construction of clean energy infrastructure such as offshore tide power and wind turbine. This paper studies the behaviour of the different cross-section and shapes of monopile under the single direction laterally load. The content of the thesis consists of five chapters. The first chapter briefly summarizes the research content and purpose as well as review and analyse the existing results. The second chapter is the laboratory experiment. The third chapter simulates the experimental data through the model established by RSPile. The experiment results show the horizontal bearing capacity of pile under different cross-sections and diameters. The fourth chapter is the data analysis and summary. This chapter checks the experimental data with the numerical simulation results. In the last chapter, the real size monopile is simulated by RSPile software. Through the data comparison in the previous chapter, the relationship between piles with different diameters and different embedded depths is summarized, and this formula is used to simulate large-diameter piles in the real world. In addition, this paper also makes a comparative test on square pile and round pile under the same soil conditions and pile materials and studies the horizontal bearing capacity of the two piles under the same horizontal load.

3. INTRODUCTION

In recent years, with the increase of people's demand for energy and the enhancement of their awareness of environmental protection, renewable energy power has developed rapidly (Kamat, 2007). Compared with traditional energy, clean energy is not only providing a low-carbon and green lifestyle for human beings, but also decreased the consuming of fossil fuel. It is a pollution-free energy supply mode advocated by modern society. The pictures below in Figures 1 and 2 are one of the main clean energies.

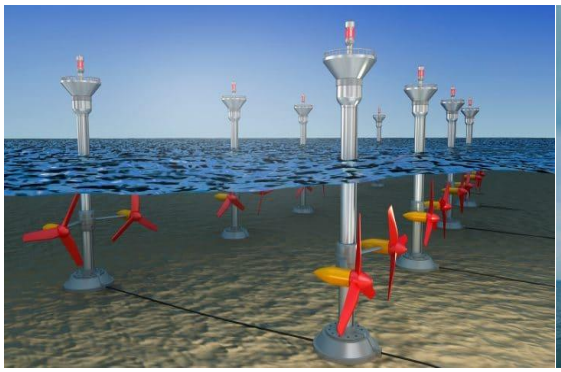

Figure 2. Offshore tide power

Figure 1. Offshore wind turbine

According to the survey of Zdravkovic et al. (2015), offshore wind power in the world is developing rapidly. In the UK alone, more than 35,000 wind turbines are being or will be installed in the next decade. In Australia, by the end of 2020, more than 2,500 wind turbines will be installed in 574 square kilometres of offshore area. These planned wind power plants will contribute 8000GWh of electricity to Australia every year (Engineers Australia 2018).

As the foundation of offshore wind power, large diameter monopile subjected to horizontal loads such as wind, wave and tide has been widely used in wind power infrastructure construction (Gavin et al. 2012). In order to make further use of the topsoil and fully mobilize the resistance of shallow soil, monopiles with different diameters, embedment depth and cross-section shapes are studied in this paper. The study content is divided into two parts. The first part carries out laboratory model experiments for monopiles, verifies the accuracy of RSPile model based on the field experimental data carried out by Murphy et al. (2016) as well as checking the horizontal bearing capacity of monopiles with different diameters, embedment depth and cross-section shapes under the laterally load. The second part uses the numerical model to

simulate the real size pile, so as to reduce the problem of high field experiment cost in the real situation.

This study case cannot only verify the rationality of RSPile numerical simulation, but also observe and analyse the pile-soil stress characteristics with the help of RSPile simulation results. It is verified that the increase of diameter can significantly improve the resistance of shallow soil and the horizontal bearing capacity of monopile from the perspectives of numerical simulation and laboratory experiment, At the same time, the laboratory experiments in the second part can also fully show the horizontal bearing capacity of monopiles with different section shapes. The research results provide reliable experimental data for guiding the design of large-diameter single piles.

4. LITERATURE REVIEW

4.1. Background.

Offshore wind power plays an important role in low-carbon energy supply. In the past decade, offshore wind power has been built on a large scale in Europe. The structural design of most offshore wind power generation devices is simple and practical. The marine environment of offshore wind turbine foundation is very different from that of land pile foundation and bears more complex loads, in which the approximate horizontal loads such as offshore wind, wave and tidal pressure (Li et al. 2013). In order to enable the top layer of those equipment to bear a variety of loads, the bottom layer structure mostly adopts pile as the foundation (Abadie et al. 2018). Because many complex forces act on a monopile, the service life of the pile is short. Ewea (2009) pointed out that the anti-lifetime of an offshore wind structure is nominally 20 to 25 years because the pile foundation is subjected to a variety of loads all year round, but this is only for reference, and the specific service life also depends on a variety of factors. Therefore, the study of pile-soil interaction is very important.

4.2. Monopile Foundations

Monopile can be divided into many kinds. According to the classification of materials, it can be divided into concrete pile, steel pile, wood pile and composite pile; According to the use function classification of pile, it can be divided into vertical compression pile, vertical uplift pile, horizontal load pile and composite load pile; According to the

section type, it can be divided into square pile and circular hollow pile. However, as the infrastructure of offshore wind power generation, pile foundation works in seawater and soil layer below the seabed all year round as well as resist various loads. Therefore, the foundation of offshore wind power generation mostly adopts large-diameter hollow steel round monopile.

Monopiles is a typical foundation option for offshore wind and tidal power facilities on shallow coast. Usually, in order to maintain the stability of the whole structure, monopiles will be penetrated into a few meters to tens of meters below the seabed (Burd et al. 2020). Due to the long length, large diameter and complex stress of the pile body, hollow steel round monopiles are mostly used in practical application.

Now most of the offshore wind turbines are developed in shallow waters, and a new wind farm in Dunkirk, UK, is completed in 2019. In this wind farm, monopile has a diameter of 7m and is designed to support a 5.5MW turbine with a water depth of 30m. (Zdravkovic et al. 2020)

4.2.1. Loading

Yegian (1973) states that since the top layer of the pile is in contact with the turbine and located above the seabed below the water surface as well as most of it is in contact with the surrounding sand and soil below the seabed, many load cases must be analysed. This includes wind load and wave load on the horizontal direction. There are variety of vertical loads react on the pile such as the self-weight and drag loads as well. Because of the complex crustal movement in offshore areas, the seabed will fluctuate under the influence of deep-sea earthquakes and tsunamis. Therefore, the force acting on the pile may also include the internal force of the soil (Hetenyi, 1946). In addition, the calculated loading is dependent on the structure's geometry and the foundation stiffness. Therefore, a certain number of load geometry iterations are required in the calculation process. Because there are too many forces acting on the pile at the same time, the types are complex. In order to avoid the interaction between various forces, this study case mainly focus on the horizontal load in one direction.

4.2.2. Wind loading effects

McAdam et al. (2018) states that the effect of wind is not only reflected in that the wind directly acts on the turbine, resulting in the stress on the lower pile, but also that the wind transmits the force to the soil around the pile through the stress structure, resulting in the interaction between the pile and soil, thus deriving the effect of rock and soil on the pile.

Arany et al. (2017) states that wind loads of different intensities are also one of the ranges to be considered in the calculation. When designing offshore wind turbines, wind loads of different intensities are usually designed according to requirements. Li (2015) adopted 50-year load and load effect for wind load calculation when designing a wind power generation facility located in the southeast coastal area of China. Similarly, Lee (2012) observed wind speed in the northeast coast of the UK. Table 1 shows the wind environmental conditions of the observation site.

Table 1. Wind environmental conditions

Environmental conditions	Hub-height 20-year	Hub-height 50-year	Hub-height 100-year
Extreme 10 min mean wind	22.0 m/s	48.7 m/s	96.3 m/s
Extreme 5s gust	28.1 m/s	57.6 m/s	104.7 m/s

4.2.3. Wave loading effects

Offshore pile foundation is different from pile foundation on land. This is because the former will be affected by wave load. Matlock (1974) observed that the frequency of sea waves is between 0.04hz-0.1 Hz, and the maximum wave frequency recorded can reach 0.05hz-0.5hz. This means that high-frequency wave load will cause relative displacement and rotation between the pile and seabed as well as cause sustained and serious damage to the monopile.

Christian (2009) also states the complexity of wave load calculation, which is not only the calculation of hydrodynamics, but also the change of tide in the calculation process. Because it will change the depth of monopiles below the water surface. In addition,

wave moves relative to pile, which means that wave will produce irregular force and apply it to the pile circularly, affecting the pile-soil stability.

4.3. Existing Analysis Methods

4.3.1. P-y curves

The p-y curve is the numerical model used to simulate the response of soil resistance (p, soil resistance per unit length of the pile) to the pile deflection (y) for the piles under lateral loading. McClelland and Focht (1956) first proposed the p-y curve method. Through the indoor soil consolidation undrained triaxial test, the relationship between the measured reaction force and displacement of the test pile should be obtained. A method for calculating the nonlinear lateral resistance of the pile, that is, the soil resistance, is proposed. Matlock (1970) carried out a large number of laterally load tests on soft clay piles and put forward the p-y curve formula of soft clay under horizontal load. Its load conditions include static loading, cyclic loading and loading after unloading. Reese and Cox (1974) carried out horizontal load pile test in sandy soil and hard clay respectively, and established p-y curves of sandy soil and dense clay. Among them, p-y curves of sandy soil are determined by parameter sand friction angle and soil reaction modulus coefficient. The p-y curve of sandy soil and hard clay proposed by Matlock and Reese fully considers the nonlinearity of soil and is selected by American Petraleum Institute (API).

The sand p-y curve proposed by Reese (1974) consists of three parts, and its structural form is complex. Later, through full-scale pile test and model test, some scholars believe that the structural form of sandy soil p-y curve should be composed of hyperbolic line segment and straightness. Others believe that the p-y curve of sandy soil is hyperbolic through model test. O'Neil and Murchison (1977) used the arctangent function to describe the curve of elastic and plastic transition zone in the p-y curve according to the experimental results. The experimental results show that the working behavior of pile foundation calculated by this p-y curve is basically consistent with the experimental results. This method is also selected by the American Petroleum Association specification (API). Ashour and Norris (1982) proposed a method of constructing p-y curve by wedge theory, namely wedge strain theory (SW), which obtains p-y curve through iterative calculation. This method is quite different from the

previous p-y curve method, which takes into account the bending stiffness and cross-sectional area of the pile.

4.3.2. P-y Curves in Cohesionless Soil

P-y curve method is a kind of elastic-plastic foundation reaction method. It considers the nonlinearity of soil and can be used for large deformation analysis of horizontal bearing pile. The p-y curve established according to model test or field test data can consider the interaction between pile and soil and the interaction between different soil layers. P-y curve method can objectively reflect the bearing deformation behavior of laterally loaded monopile. Therefore, it has been widely used in recent years. How to construct p-y curve is the key to the application of p-y curve method.

Reese et al. (1976) based on the field test results, established the p-y curve of multi-stage linear of straight pile in sand. O'Neill and Murchinson (1983) compared various p-y curves of straight piles in sand and considered that hyperbolic tangent function can be used to describe p-y curve. Based on Coulomb passive earth pressure theory, Zhang et al. (1993) modified the ultimate soil reaction and initial foundation reaction modulus of vertical pile in sand proposed by Reese et al. (1976) and established the p-y curve of inclined pile. It can be seen from the above analysis that the p-y curve method is one of the methods recommended in the current code to calculate the horizontal bearing capacity of pile foundation. The response of soil under transverse load can be expressed by the stress displacement curve (p-y curve) of soil along the depth. The p-y curves at each depth do not interfere with each other and form a curve cluster to express the stress-strain state of pile-soil system.

Image removed due to copyright restriction.

Figure 3. Typical p-y curves (Reese et al. 1974)

4.3.3. P-y Curves in Cohesion Soil

According to the p-y curve method, the nonlinear relationship between resistance p (kN / m) and displacement y (m) of unit length soil can be determined according to the actual situation of soil along each depth of pile body. The p-y curve method can not only consider the nonlinear interaction between pile and soil, soil stratification, different load forms (such as static load and cyclic load), but also introduce the effect of soil weakening, degradation and reduction of soil resistance on the mechanical behaviour of pile. Therefore, the p - y curve is of great significance for the analysis of laterally loaded piles

Matlock (1978) analysed the stress condition of laterally loaded pile in clay by using clay p-y curve:

$$y/y_{50} < 8, p/p_u = 0.5(y/y_{50})^{1/3} \quad (1)$$

$$y/y_{50} < 8, p/p_u = 1.0 \quad (2)$$

Where P_u = Ultimate resistance of soil per unit length

y_{50} = When the soil reaches half of the ultimate horizontal resistance, the lateral deformation of the pile at the corresponding depth.

$$y_{50} = \eta \varepsilon_{50} d \quad (3)$$

where η = Empirical coefficient, generally, take η= 2.5

ε_{50} = The axial strain corresponding to the principal stress difference reaching half of the maximum principal stress difference in triaxial shear test

d = Pile diameter.

Image removed due to copyright restriction.

Figure 4. P-y curve for clay (Matlock 1970)

4.3.4. Limitation of p-y curve analysis

Although the p-y curve model can well reflect the ground nonlinearity of soil, in recent years, with the increase of pile diameter of offshore wind power single pile foundation, the slenderness ratio of pile foundation decreases. Wiemann (1994) found that for rigid piles with small slenderness ratio, the p-y curve has the defect of overestimating the initial foundation stiffness; With the increase of depth, the initial foundation stiffness is overestimated more seriously. Therefore, the design of offshore wind power single pile foundation is too conservative, increasing construction and operation costs. Ashford et al. (1996) carried out the horizontal vibration test of pile foundation, found that the initial foundation stiffness is related to the relative stiffness of pile and soil, and revised the calculation method of initial foundation modulus; The results show that the natural vibration frequency of pile foundation calculated based on the foundation reaction modulus recommended by Terzaghi is in good agreement with the measured results. Abdel-Rahman (1997) and Sorensen et al. (1999) shows that the p-y curve method underestimates the horizontal displacement of pile top under extreme load. Kelleher et al. (2000) corrected the initial stiffness of p-y and applied it to the calculation of a wind farm. The results show that the pile diameter has a significant effect on the initial foundation stiffness between pile and soil. The research results of Ousmane et al. (2001) once again show that there are defects in the initial foundation stiffness in the current p-y curve. Achmus et al. (2003) combined with previous studies,

discussed the applicability of the current p-y curve and considered that the influence of the pile diameter changing on the initial foundation modulus cannot be ignored.

4.3.5. Numerical Analysis

Finite element method is a powerful numerical method. It is a numerical analysis method that discretises complex objects reasonably and solves complex problems by using mechanics and computer technology. The application of finite element to pile foundation analysis began in the 1970s. After decades of development, many algorithms have been formed, and its theory is becoming more and more rich and perfect. Many problems that cannot be solved by other methods have been successfully solved. The numerical simulation of pile-soil interaction has attracted more and more attention of civil workers, and its research is also showing a very active scene. At present, it has become the mainstream of pile foundation analysis.

In the final analysis, two basic problems need to be solved in the numerical analysis of pile-soil interaction: one is the research on the linear and nonlinear constitutive model of soil; The second is the description of the constitutive relationship on the pile-soil contact surface and the selection of contact elements. The commonly used soil constitutive models include generalized hook law, Duncan Chang model, Mohr Coulomb model, modified Cam clay model, etc; The common contact surface elements include Goodman interface element with or without thickness, Desai thin layer interface element, Yin (1981) contact surface element with thickness, Katongga (1983) constraint element, etc. the selection of which model should be considered according to the specific engineering practice.

The diversity of large-scale finite element analysis software provides favourable conditions and convenient ways for the numerical simulation of pile-soil interaction. For example, when using the large-scale finite element analysis software ABAQUS to analyse pile-soil interaction, the conventional calculation method based on p-y curve method is to simplify the pile-soil interaction into a spring element related to horizontal, vertical and torsional characteristics.

ABAQUS analysis software has been widely used in civil engineering, geology and minerals, hydraulic engineering, marine engineering and other fields, and has become the mainstream of simulation analysis software in civil construction industry. The software mainly includes three modules: pre-processing, analysis and calculation and

post-processing. It can easily use the pre-processing module for modelling and mesh generation, and then use the analysis types (linear analysis, nonlinear analysis, transient, modal, etc.) in the calculation and analysis module for finite element calculation. Finally, the calculation results can be viewed or extracted through the post-processing module.

The data processing process of the calculation results of large-diameter pile with ABAQUS software is as follows:

（1） Extract the tensile strain of pile section at each specified depth ε_T and compressive strain $\varepsilon_{T。}$

（2） Calculate the corresponding section curvature Φ

$$\emptyset(z) = \frac{\varepsilon_{(T)}(z) - \varepsilon_{(C)}(z)}{D} \tag{4}$$

（3） Calculate the bending moment M

$$M(z) = EI\emptyset \ \ (\mathrm{z}) = K\frac{\varepsilon_{(T)}(z) - \varepsilon_{(C)}(z)}{D} \tag{5}$$

Where E = Elastic modulus of pile

I = Moment of inertia

K = Flexural stiffness, (K=EI)

D = Calculated width

（4） Fitting the relationship between bending moment and depth Z

（5） According to the relationship fitted in step (7), the soil resistance P at the pile side is calculated from equation (6)

$$p(z) = \frac{d^2\mathrm{M}_{(T)}}{EIdz^2} = \frac{d^2\emptyset_{(T)}}{dz^2} \tag{6}$$

（6） According to the fitting relationship in equation (7), calculate the pile lateral displacement y from equation (7)

$$y(z) = \iint \frac{\mathrm{M}_{(z)}}{EI} dz^2 = \iint \emptyset(z) dz^2 \tag{7}$$

4.4. Limitations of research

In addition to the advantages of wide universality, high precision and strong modelling ability, the finite element also has the ability to obtain the stress-strain relationship of soil medium around the pile. It can well simulate the nonlinear characteristics of soil such as consolidation, seepage, hardening and creep. It overcomes the defect that the traditional analytical method simplifies the soil to an elastic state and cannot well simulate the pile-soil contact relationship. Moreover, the accuracy of numerical analysis can be controlled to a certain extent, and the forms and ways are relatively unified. It is a numerical analysis method with good programmability. Therefore, the finite element method is an effective method to study the characteristics of single pile and pile group under vertical load and horizontal load, as well as the interaction between pile and soil. The disadvantage of finite element method is that the solution is more complex, especially for three-dimensional analysis. the problem of difficult convergence and long machine time is particularly prominent, and the rationality and accuracy of the solution are greatly affected by the selection of modelling methods and parameters.

5. METHODOLOGY

The most important two parts in this study are experimental analysis and the numerical analysis. The flow chart is shown in the Figure 5.

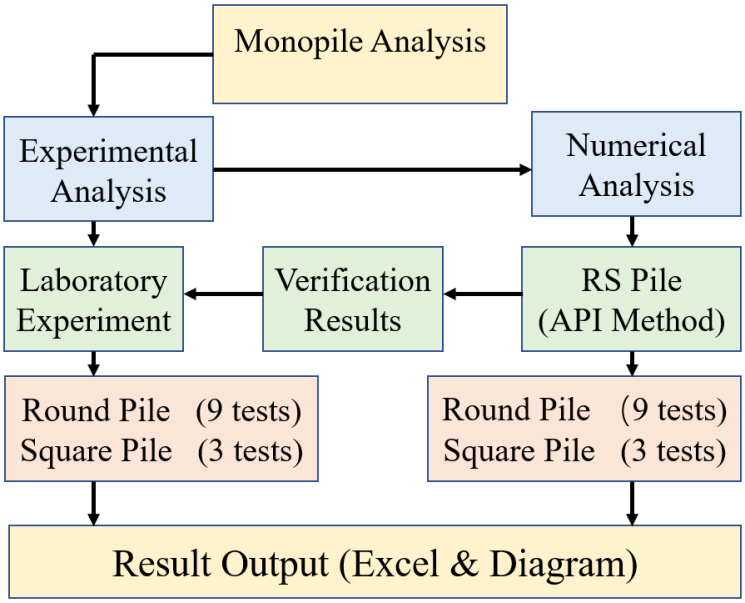

Figure 5. Methodology process

5.1. Experimental investigations

In order to investigate the response of pile under horizontal load, a series of experiments were carried out in the Civil Engineering Laboratory at the Tonsley campus of Flinders University. Field experiments can get the most accurate results, but due to the limitations of test cost and field conditions, it is difficult to carry out comparative experiments. The model test uses a small-scale model to simulate the real size and has the advantages of easy control of the experimental process, repeatability of the experiment and easy adjustment of the characteristics of foundation soil. Therefore, it is widely used and more and more used to explore the feasibility of new foundation. For the large diameter monopile foundation of offshore wind power, there are the above problems that it is difficult to carry out full-scale experiments and the cost will be expensive. Therefore, for the large-diameter single pile in offshore wind power foundation, 12 groups of horizontal load model experiments are designed to study the effects of pile diameter, embedment depth, cross section and other factors on the horizontal bearing capacity of single pile foundation, The response of large-diameter pile under real load is deduced through later numerical simulation.

5.1.1. Sand Properties

The dry medium coarse quartz sand is selected for this experiment. The uniformity coefficient C_u and coefficient of curvature C_c of sand are 3.1 and 0.74 respectively. According to the experimental requirements, the unit weight of dense sand is 16.7 ± 0.02kN/m^3. In addition, the internal friction angle of sand is 30 °. Figure 6 shows the particle size distribution of sand and Table 2 shows the physical properties of sand.

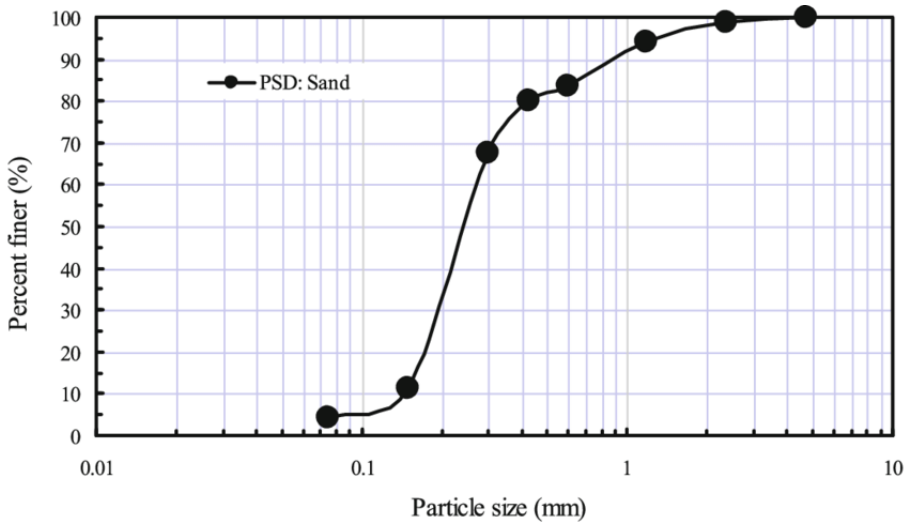

Figure 6. The particle size distribution of sand

5.1.2. Model piles

This experiment takes the pile foundation of offshore wind power plant as the prototype to carry out 12 groups of comparative model tests. The prototype pile in this experiment is a large diameter monopile with a diameter of 5.4m. Among them, 12m on the soil surface and 24m underground. Steel pipe pile is used, with elastic modulus of 210GPa and Poisson's ratio of 0.28. The model is simulated by hollow pile with equal section and steel, which is similar to the bending stiffness of prototype pile. According to the material mechanics, the pile bending moment:

$$EI = E[\pi(D^4 - d^4)/64] \quad (8)$$

Where E = Elastic modulus

I = Moment of inertia, D= External diameter

d = Internal diameter

Figure 7. Model piles

According to the calculation, the pile length of the standard model pile is 1008mm, the wall thickness is 1.5mm, and the distance from the loading position to the sand surface is e = 335mm. According to the collective properties of prototype piles, four kinds of test piles are set respectively. The physical properties of piles are the same, and the details of geometric properties are shown in Figure7 and Figure8.

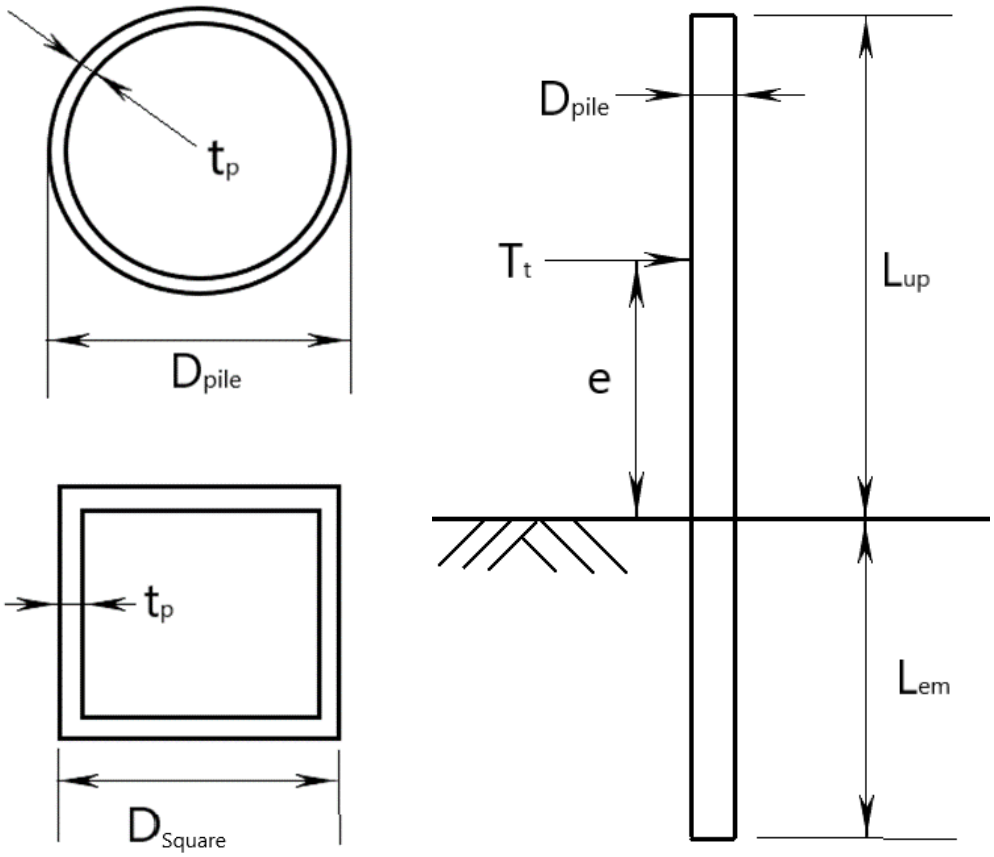

Figure 8. Geometric properties of piles

5.1.3. Test procedures

(1) Prepare model piles. Make model piles of different sizes according to the experimental requirements

(2) Dry the sand in an oven, configure the moisture content, stand for 24 hours to ensure uniform moisture.

(3) Drive the model pile vertically into the sand with a rubber hammer to the specified embedded depth.

(4) Dial gauge A and B is respectively arranged on both sides of the pile to measure the displacement change of the pile.

(5) Apply horizontal load at the load eccentricity, increase the load of each level by 0.5-1n, so that the change rate of horizontal displacement is less than 0.01mm/min.

(6) Record dial gauge, reading data, and observe model pile behaviour at the same time.

(7) After the load loading is completed, unload the load step by step and record the data until all the loads are unloaded.

(8) After loading and unloading, observe the changes of each part of the model in detail, and make analysis records.

(9) All the prepared model piles shall be used for the experiment in turn until all recording and observation work are completed.

(10) Dismantle the model, clean up the laboratory and end the test.

A total of 12 tests were set up to study the effects of pile section size, shape and length-diameter ratio on the horizontal bearing capacity of piles. Table 3 shows the test details. Figure 9 shows the instruments used in this experiment.

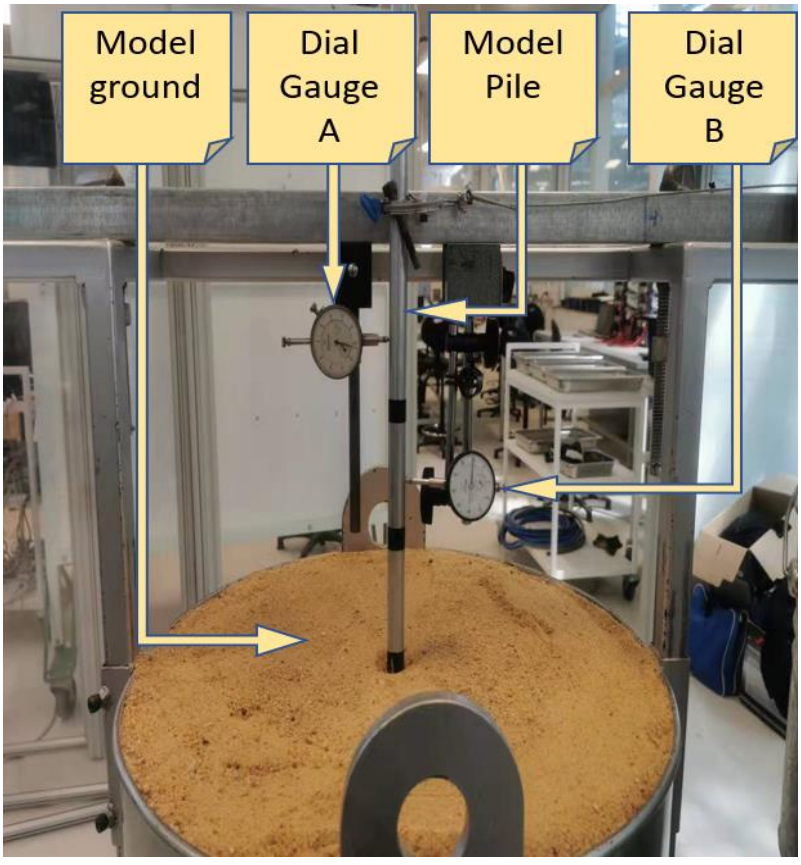

Figure 9. Test instruments

Table 2. The details of 12 groups of control experiments

Test NO.	Test 1 Round pile	Test 2 Round pile	Test 3 Round pile	Test 4 Round pile	Test 5 Round pile	Test 6 Round pile	Test 7 Round pile	Test 8 Round pile	Test 9 Round pile	Test 10 Rectangle pile	Test 11 Rectangle pile	Test 12 Rectangle pile
Pile shaft diameter or width D_{pile} (mm)	19	19	19	32	32	32	50	50	50	50	50	50
Embedment length L_{em} (mm)	200	250	300	200	250	300	200	250	300	200	250	300
Equivalent slenderness ratio (L_{em}/D_{pile})	10.53	13.16	15.79	6.25	7.81	9.38	4.00	5.00	6.00	4.00	5.00	6.00
Load eccentricity e (mm)	335	335	335	335	335	335	335	335	335	335	335	335

5.1.4. Determination method of horizontal loading capacity of monopile model

For pile-soil interaction, there are three methods to design the loading capacity

(1) The first criterion is when the load displacement curve of pile has obvious inflection point. At the initial stage of loading, the curve is in the linear stage. With the increase of load, the curve presents a nonlinear form. After the load increases to a certain value, the curve has an obvious inflection point, and then the displacement increases rapidly, resulting in the failure and instability of the pile. The load corresponding to the inflection point is determined as the bearing capacity of steel pipe pile. In this case, the steel pipe pile is damaged before the soil under the pile-soil interaction.

(2) The second criterion is when there is no obvious inflection point in the load displacement curve of the pile. The load corresponding to the point where the slope of the curve is close to zero is taken as the ultimate bearing capacity of the slowly varying curve. At this time, even if the load increment is very small, it will cause a

significant increase in displacement, indicating that the structure has been unstable and damaged.

(3) The third criterion is based on the allowable rotation angle. If the pile is less than the allowable rotation angle under laterally loads, the structure is stable. If the pile exceeds the allowable rotation angle, the soil is considered failed. The relationship between load and rotation angle can be expressed by calculation. According to the results of experiment tests, it can be recognized that the soil is failed if the pile angle exceeds 3 °.

According to the shape of the curve and the allowable displacement, the small value of the load determined by each method is taken as the final horizontal bearing capacity of the large diameter monopile. In this case study, due to the small size of the pile, the depth of the pile embedded in the soil is shallow, and the force exerted on the pile is small. Therefore, soil failure is defined as when the rotation angle of the pile exceeds 3 °.

5.1.5. Test results

The 12 model tests adopt similar methods to process the experimental results, visually analyse the load step by step and the data read after the test and then use the formula in the diagram below to convert the load and the displacement and rotation angle of the pile to obtain the horizontal load horizontal displacement curve. Test 9 is taken as an example to illustrate the comprehensive analysis.

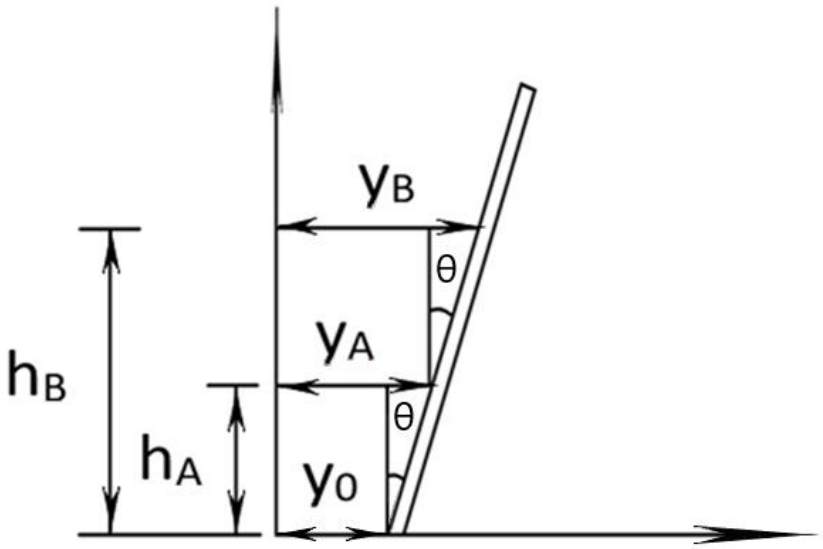

Figure 10. Displacement calculated modelling process

$$tan\theta = \frac{y_B - y_A}{h_B - h_A} \quad (9)$$

$$y_0 = y_A - h_A tan\theta \quad (10)$$

Where θ = Rotation angle

y_0 = Pile displacement

Test9 is a single pile model test with hollow round section. The length section diameter ratio (L_{em} / D) of the pile is 6.0. The pile is embedded in the soil to a depth of 300mm. (Note: the pile length L means the length from the load act point to the bottom of the pile). Firstly, as shown in Figures 11,12 and13, after each load, the pile displacement is measured intuitively by manual measurement to observe the displacement change of the pile, and then the horizontal load horizontal displacement curve is drawn according to the dial gauge readings on both sides of the pile. The analysis shows that the loading device can work normally during the operation of the experimental device, and the pile top deflects step by step with the increase of horizontal load.

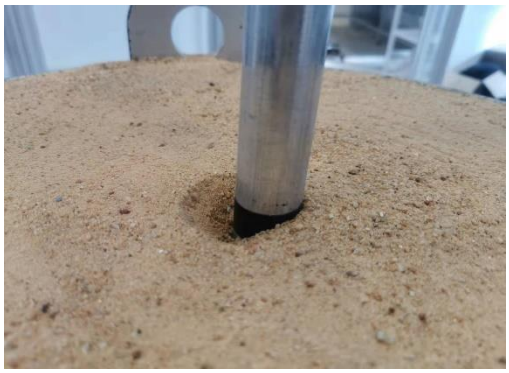

Figure 11. Soil failure

Figure 12. Manual measurement

Figure 13. Dial measurement

Figure14 shows the horizontal load-displacement curve. The analysis shows that a total of 13 levels of laterally load are applied. With the gradual increase of laterally load, the pointers of two dial gauge deflect obviously, and the horizontal displacement increases gradually. During the experiment, the maximum load is 260N and the maximum horizontal displacement is 5.61mm. The original experimental data is shown in Table 7 in appendix.

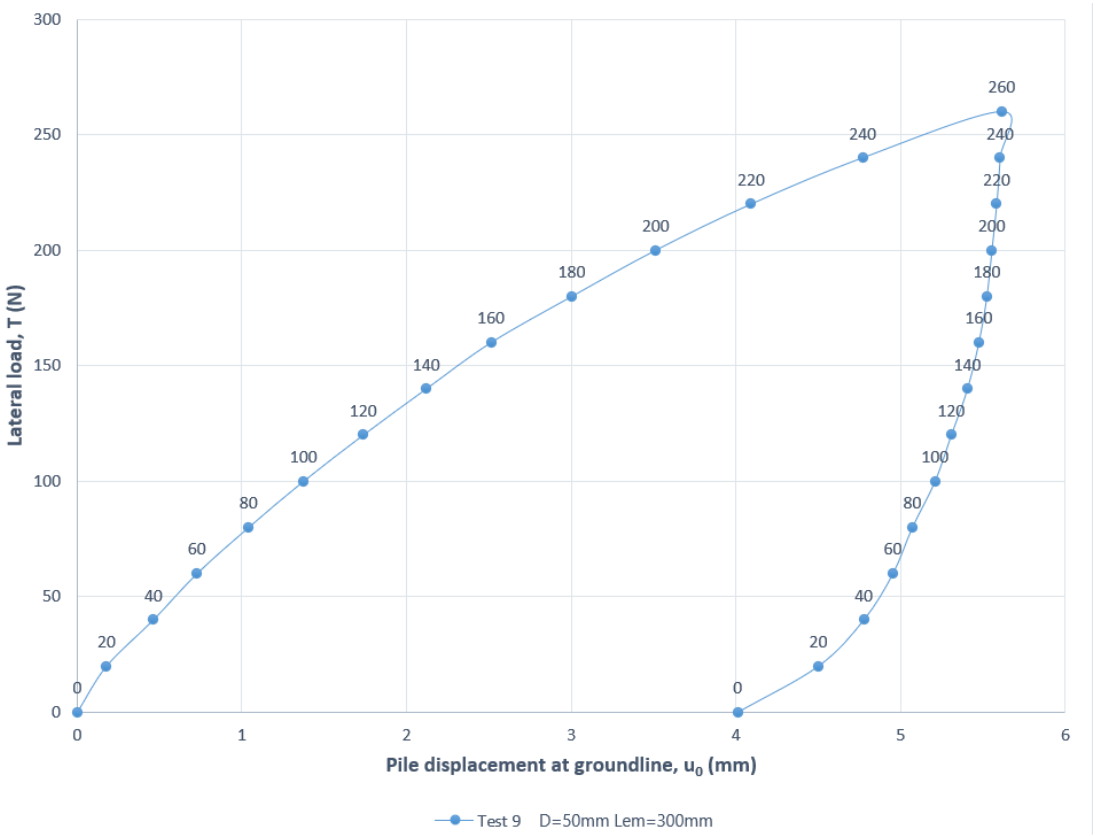

Figure 14. The horizontal load horizontal displacement curve

5.1.6. Result Analysis

The horizontal bearing capacity of monopile is compared and analysed from the buried depth, diameter and cross section shape. The Figure15 and 16 show both displacement and bending moment data.

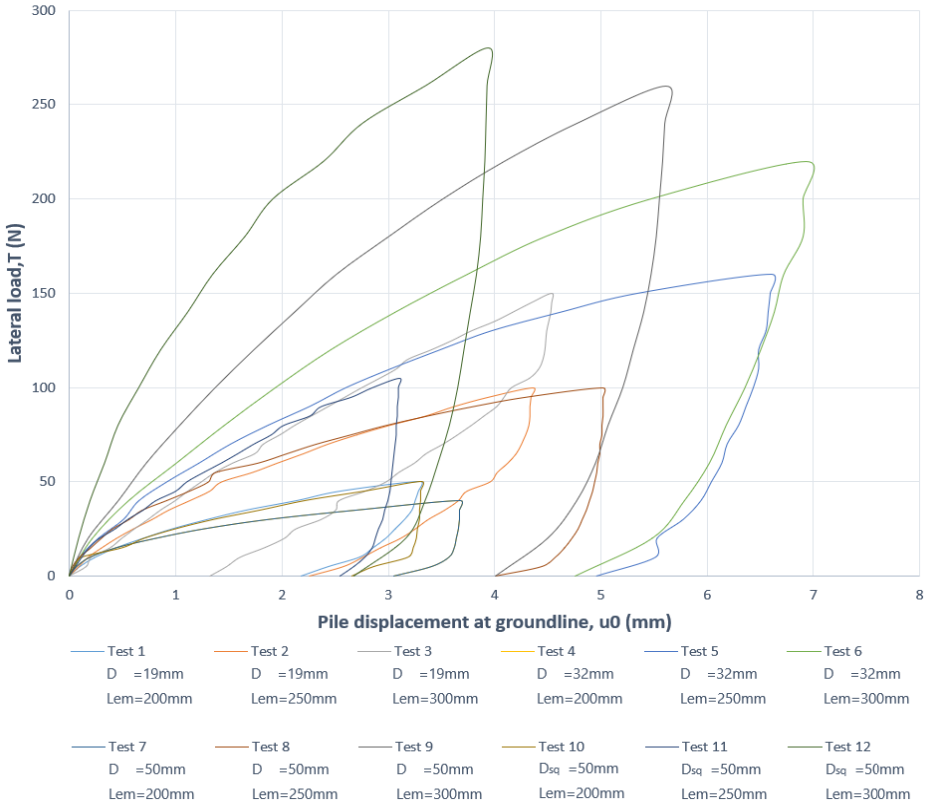

Figure 15. Load-displacement experimental results

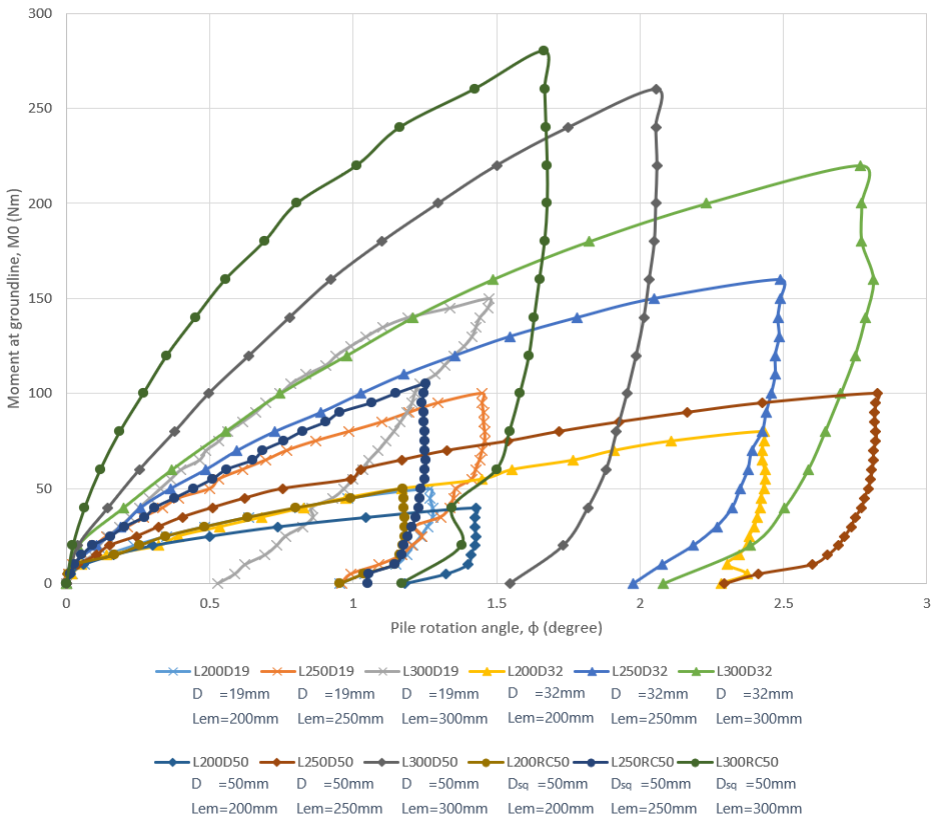

Figure 16. Moment-rotation experimental results

(1) Effect of Pile embedded depth

Figure 17 shows the load-displacement curves of tests 7, 8 and 9. The analysis shows that the depth of pile embedded in soil, and the horizontal bearing capacity of single pile is significantly improved. Taking the horizontal load 40N as an example and taking the horizontal displacement of the pile in test 9 as the reference, the horizontal displacement of the pile in test 8 and test 7 are 1.97 times and 8.78 times respectively.

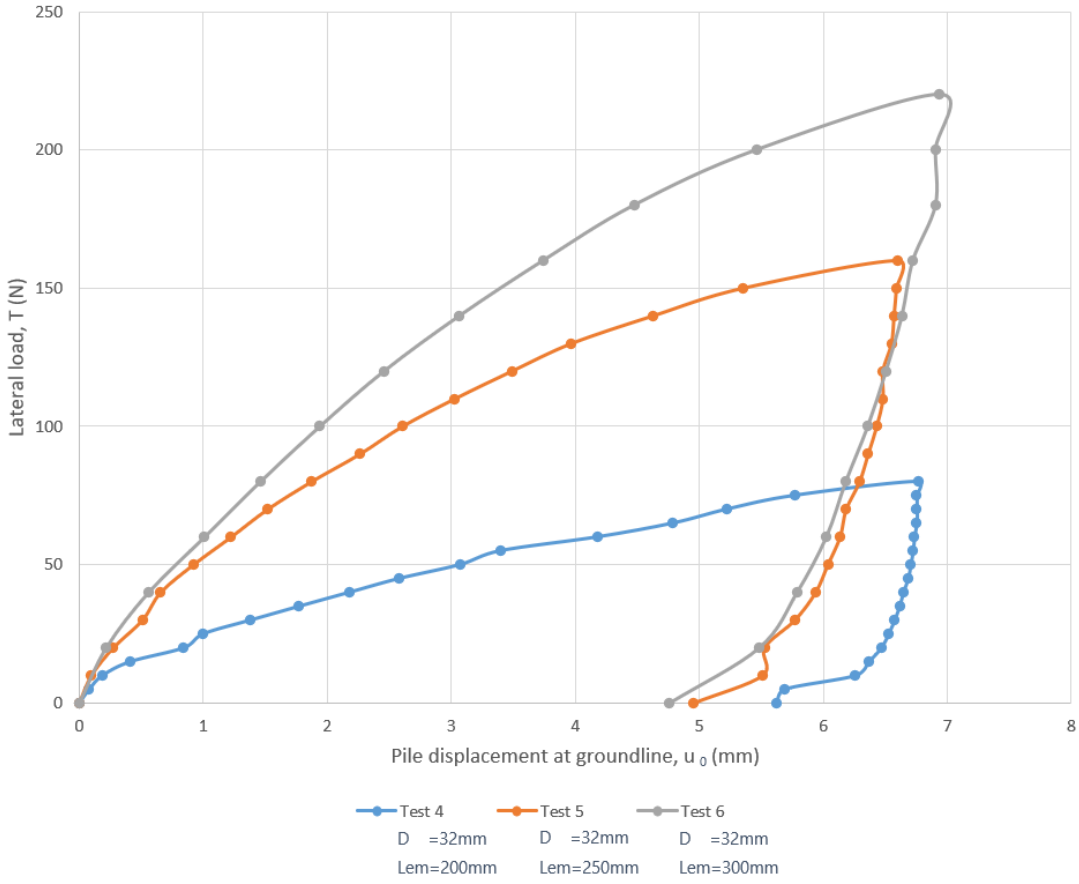

Figure 17. The horizontal load horizontal displacement curves of test 7, 8 and 9

(2) Effect of pile diameter

Figure 18 shows the load-displacement curves of tests 3, 6 and 9. The analysis shows that the diameter becomes longer and the horizontal bearing capacity of a single pile is significantly improved. Taking the horizontal load 140N as an example, taking the horizontal displacement of the pile in test 9 as the reference, the horizontal displacement of the pile in tests 3 and 6 are 1.45 times and 1.96 times respectively.

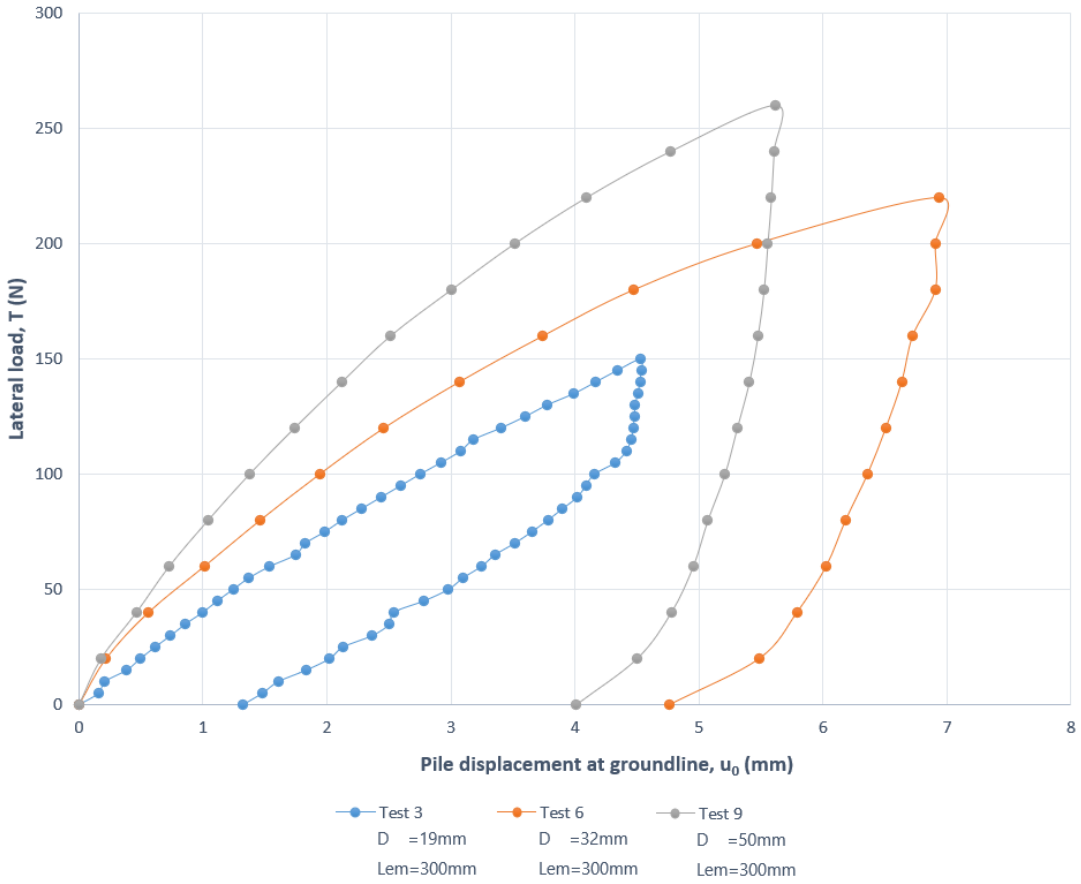

Figure 18. The horizontal load horizontal displacement curves of Tests 3, 6 and 9

(3) Effect of pile cross section shape

The load-displacement curves of tests 9 and 12 are shown in Figure 19. The analysis shows that the displacement of rectangular section pile and circular section pile with equal side length and diameter is less than that of the latter under the same horizontal load. Taking the horizontal load 160N as an example, taking the horizontal displacement of the pile in test 12 as the reference, the horizontal displacement of the pile in test 9 is 1.86 times.

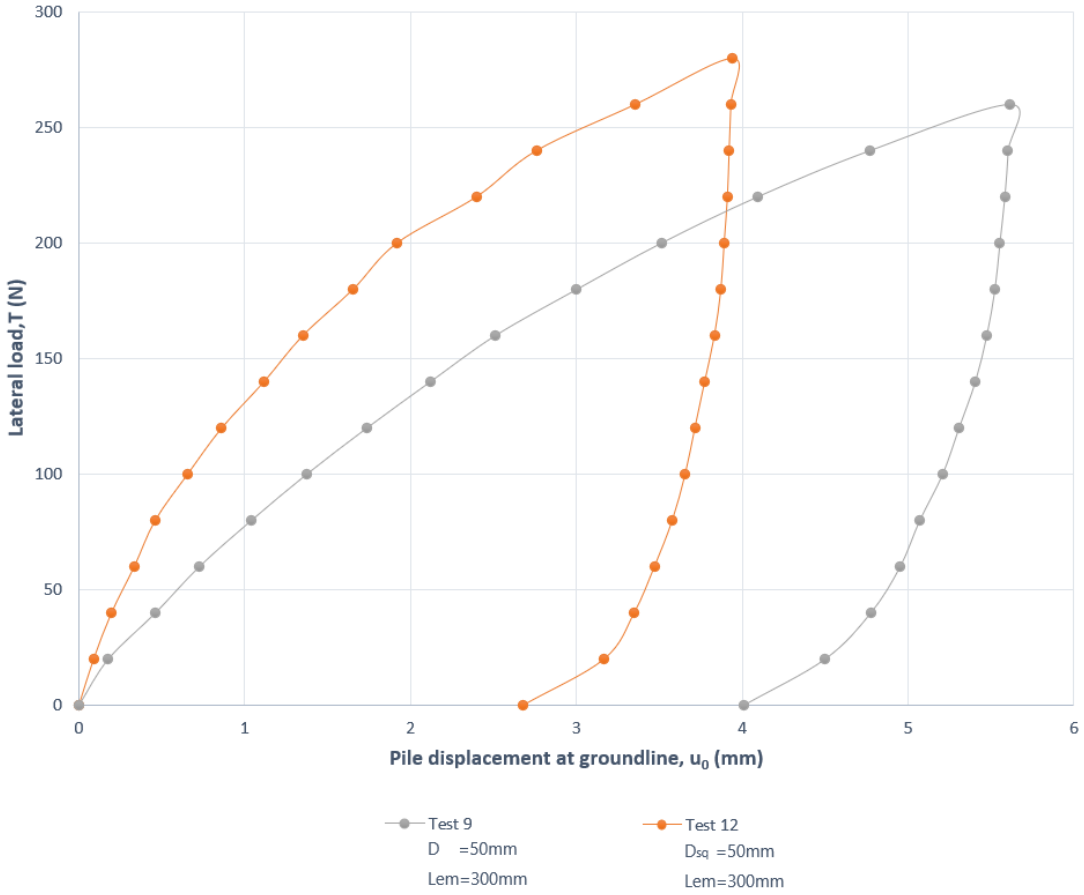

Figure 20. The horizontal load horizontal displacement curves of tests 9 and 12

(4) L_{em} / D range results

Figure 20 shows the load-displacement curve of tests 1,2 and 3. Byrne (2015) pointed out that the range of L_{em} / D should be controlled within the range of 3-8. The analysis shows that in the model experiment, when L_{em} / D exceeds the range of 3-8, the reduction of load will not lead to the change of pile displacement in the initial stage of load unloading. Taking the horizontal loads of 150N and 120N as examples, when the load is reduced from 150N to 120N in test 3, the horizontal displacement of the pile is only reduced by 0.07mm.

Table 3. L / D ratio of all circular section piles

L_{em}/D_{pile}= 3-8 (Byrne, 2015)	Test 1	Test 2	Test 3	Test 4	Test 5	Test 6	Test 7	Test 8	Test 9
L_{em}/D	10.5	13.2	15.8	6.3	7.8	8.0	4	5	6

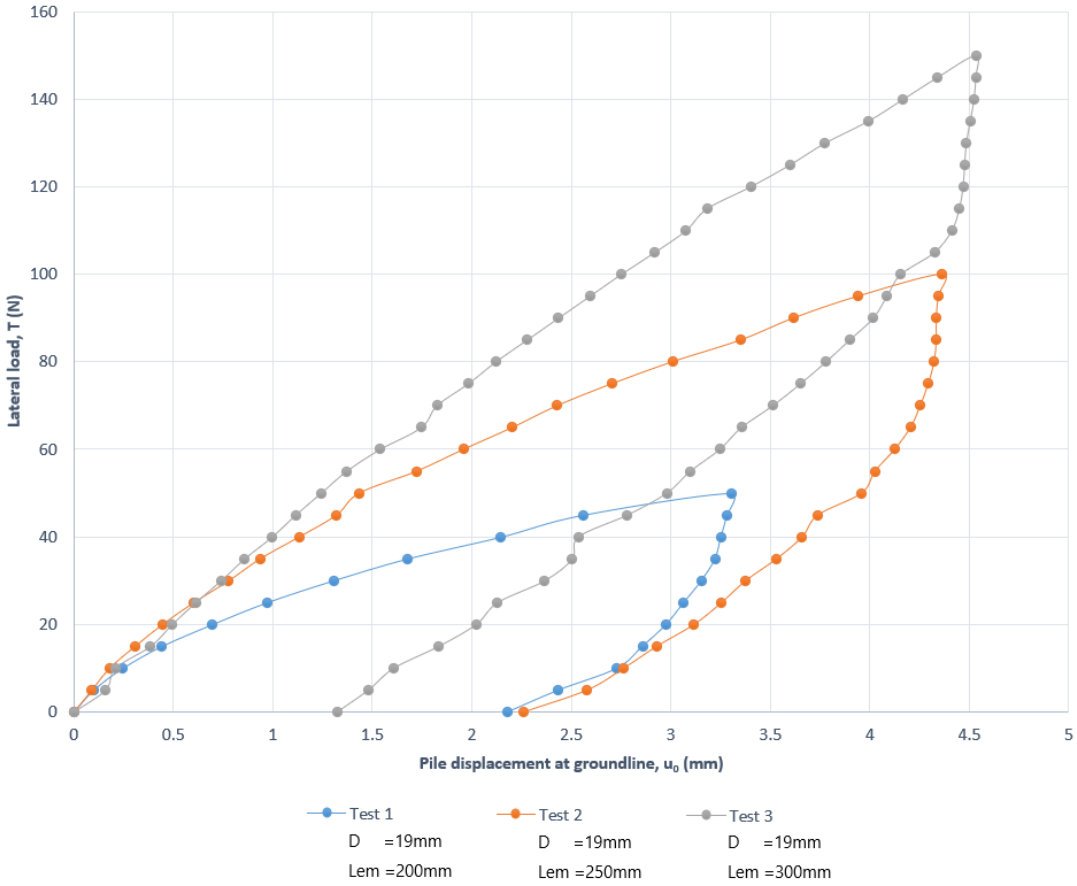

Figure 21. The lateral load - displacement curve of tests 1,2 and 3

Liang (2012) stated that if the L_{em}/D in the range of 3-8, the pile will present a rigid structure. The vertical additional stress around pile can be presented as:

$$\sigma_z' = \sigma_s e^{-\frac{u}{A-A_p}K_z \tan\varphi'} - \frac{c'}{K\tan\varphi'}\left(1 - e^{-\frac{u}{A-A_p}K_z \tan\varphi'}\right) \qquad (11)$$

$$K = 1 - sin\varphi \tag{12}$$

$$L_0 = \frac{A-A_p}{uKtan\varphi'} ln(1 + \frac{\sigma_s K tan\varphi'}{c'}) \tag{13}$$

Where σ_z' = Vertical additional stress of soil between piles at depth z

u = Pile perimeter

A = Area borne by a single pile

A_p = Area of cross section

K = Earth pressure coefficient of soil between piles acting on pile side

z = Calculate depth

c' = Cohesion between pile and soil

φ' = Friction angle between pile and soil

L_0 = Z distance to pile top

According the equations (11) and (13) and the experiment data, the relationship between vertical additional stress of piles and depth is shown in Figure 22.

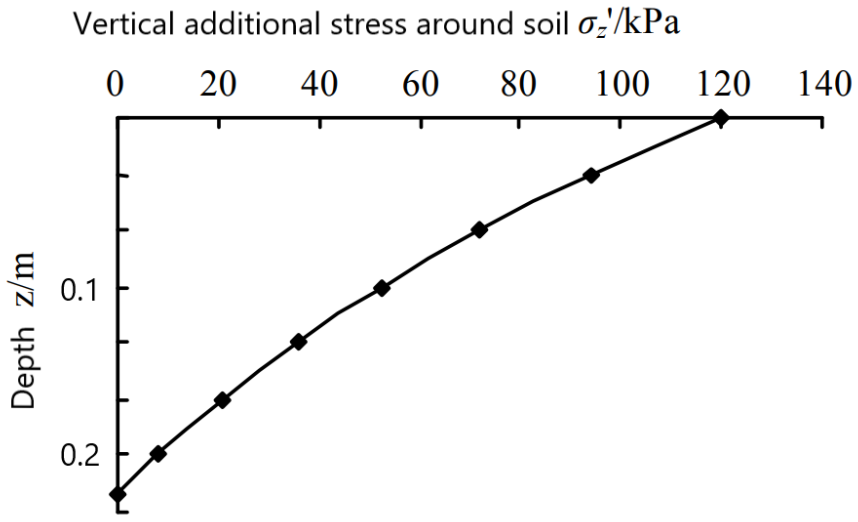

Figure 22. The relationship between vertical additional stress of piles and depth

5.2. Numerical Analysis

With the improvement of numerical analysis technology, it is very common to calculate and analyse the structural characteristics through numerical simulation. While carrying out the model experiment, this thesis tests the experimental data by using RSPile software, summarizes the function law through the data, and finally carries out the numerical simulation of the real size pile diameter through the obtained function, so as to solve the problem that the field experiment cannot be carried out in the actual engineering problems.

This part is divided into four parts. The first part verifies the accuracy of the model established by RSPile through the field experimental data of other scholars. The second part uses the validated RSPile model to check the previous model experiments. The third part summarizes the experiment through RSPile and studies the relationship between pile-soil interaction. The last part is the numerical simulation of normal size pile-soil structure in the real world through the summarized functional relationship.

5.2.1. RSPile introduction

Rspile is a general pile foundation analysis software, which is suitable for analysing driven pile, axial pile and lateral pile. It can calculate the axial bearing capacity of driven pile under various loads and soil displacement, as well as the internal force and displacement of pile.

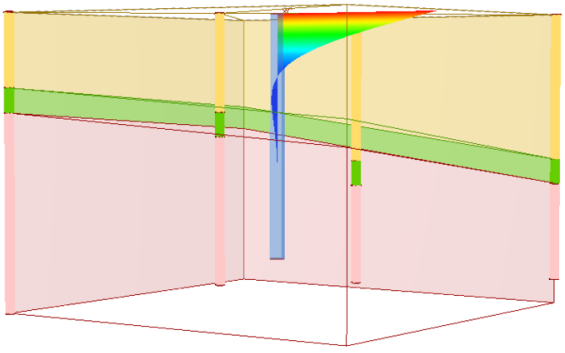

Figure 23. 3D view of RSPile modelling

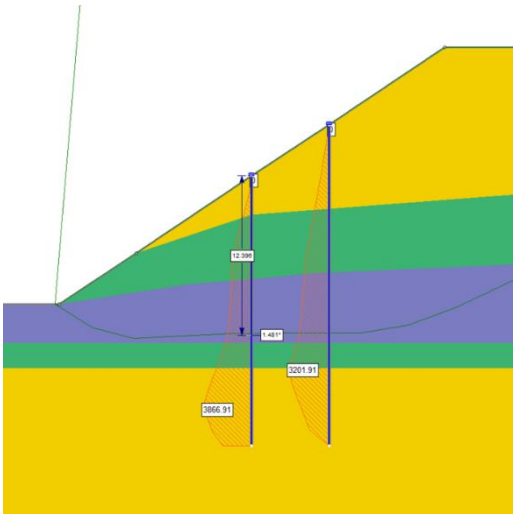

Figure 24. 2D view of RSPile modelling

5.2.2. Theory

RSPile model calculation is based on p-y curve method. In order to correctly analyse the lateral load pile foundation in sand, a nonlinear relationship needs to be applied to provide soil resistance as a function of pile deflection. Figure 25-A shows a round pile under laterally load. As shown in Figure 25-B, after unloading, the unit stress perpendicular to the pile is evenly distributed. When the pile deflects a distance y_1 at the depth of z_1, the stress distribution is similar to Figure 25-C. When the resistance is p_1, the stress on the backside of the pile decreases and the stress on the front increases. When the displaced soil tries to move around the pile, some unit stresses include normal and shear components.

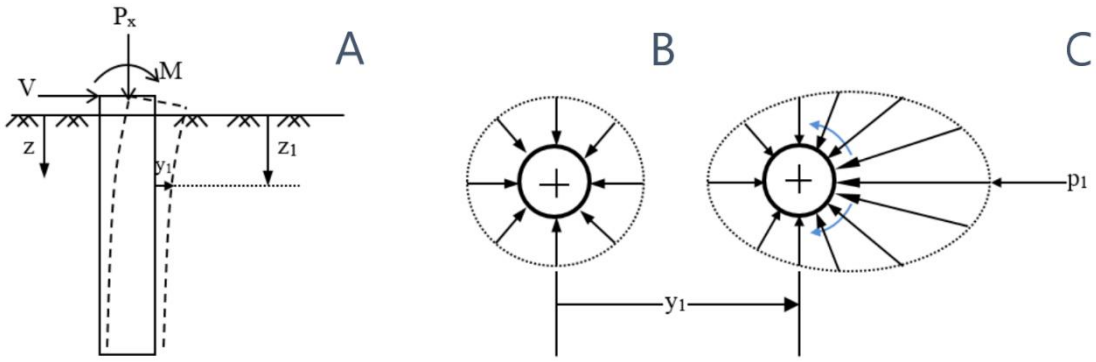

Figure 25. Unit stress distribution of pile under laterally load

Hetenyi (1946) derived the differential equation is used to solve the pile-soil interaction by p-y curve method. The conventional form of the differential equation is given by equations (11)-(14):

$$E_p I_p \frac{d^4y}{dx^4} + P_x \frac{d^2y}{dx^2} + E_{py}y - W = 0 \quad (11)$$

$$E_p I_p \frac{d^3y}{dx^3} + P_x \frac{dy}{dx} = V \quad (12)$$

$$E_p I_p \frac{d^2y}{dx^2} = M \quad (13)$$

$$\frac{dy}{dx} = S \quad (14)$$

Where y = Lateral deflection of the pile,

E_pI_p = Bending stiffness of pile,

Px = Axial load on pile head,

E_{py} = Soil reaction modulus based on p-y curves,

W = Distributed load down some length of the pile,

V = Shear in the pile, M=Bending moment of the pile,

S = Slop of the curve defined by the axis of the pile.

5.2.3. Modelling

The single pile of large-diameter steel pipe pile adopts linear elastic model, with elastic modulus E = 200GPa, Poisson's ratio μ= 0.28 and density ρ= 1670kg / m^3. P-y curve model is adopted for soil. The small diameter pile model is established through RSPile software, and the model inspection includes three static analysis steps:

(1) Set boundary conditions and add model properties
(2) Set up soil model and input soil parameters
(3) Set up the pile model and enter the parameters of the pile
(4) Apply soil gravity, in-situ stress balance and pile gravity
(5) Apply laterally load
(6) Adjust the data to make the results consistent with the experimental results
(7) Export data

In RSPile, in order to simulate the real situation that the soil has stress contact without displacement under gravity, it is necessary to balance the in-situ stress of the soil. RSPile provides setting options that can be directly used for in-situ stress balance.

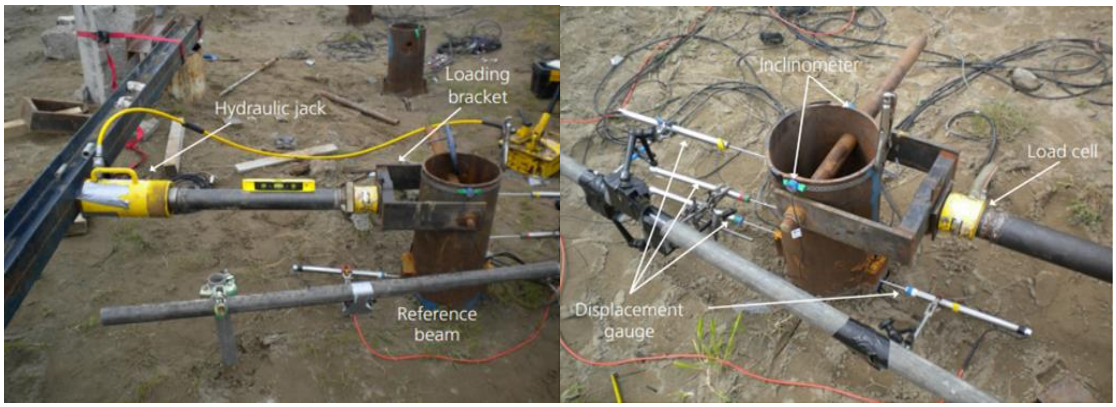

Figure 26. Field tests (Gerry 2016)

Figure 26 shows all field test equipment by Gerry (2016). Both Tables 4 and 5 represent the value of soil and pile properties. The curve in Figure 29 represents the case for 30kN laterally loaded model pile behaviour and diagrams A to D present the relationship of depth, bending moment, shear force, rotation and displacement under the field test data by Gerry (2016). Gerry (2016) used three types of piles in the field test. One is about the round pile (RP) and the other two are about wing pile (WP1 and WP2). In this study, all of investigation about the monopile, therefor, only consider the round pile (RP) result with Gerry (2016) works.

Table 4. Soil geotechnical properties (Gerry 2016)

Soil property	Blessington test site	Garryhesta test site
Average cone tip resistance, q_c	9·88 MPa	6·65 MPa
Peak friction angle, ϕ'_p	42° at 0·5 m, 44° at 2 m	45° at 0·5 m, 40° at 2 m
Constant volume friction angle, ϕ'_{cv}	36·5°	33°
Relative density, R_d	≈100%	≈70%
Coefficient of lateral earth pressure, K_0	2·5 at 0·5 m, 1·5 at 2 m	2·2 at 0·5 m, 1 at 2 m
Bulk unit weight, γ'_b	20 kN/m^3	18·6 kN/m^3
Overconsolidation ratio, OCR	20 at 0·5 m, 10 at 2 m	15 at 0·5 m, 5 at 2 m
Small strain shear stiffness, G_0	150 MPa	200 MPa
Moisture content	≈12%	≈12%
Percentage fines	4–13%	6–16%
Soil classification	Dense silty sand	Very silty sand SM

Table 5. Pile properties (Gerry 2016)

	Units	Reference pile (RP)	Wing 1 (WP1)	Wing 2 (WP2)
Length, H	mm	2000	2000	2000
Embedded length, L	mm	1500	1500	1500
Diameter, D	mm	244·5	244·5	244·5
Wall thickness	mm	8	8	8
Wing width, b_w	mm	NA	185	185
Wing length, h_w	mm	NA	280	560
Wing thickness	mm	NA	8	8
Additional steel[a]	%	NA	14	28

RSPile is used for numerical simulation analysis of field experiment. A comparison of the Figures 27 and 28 demonstrates dramatically the influence of lateral load. Under the 40kN lateral load in Figure 27, the maximum bending moment of RSPile appears the depth between 0.42m to 0.46m and the field test has the similar data. Similarly, it can be seen from the Figure 28 that both RSPile and field test results have the similar

results under the 30kN laterally load as well as the same tend. Therefore, RSPile meet the modelling accuracy.

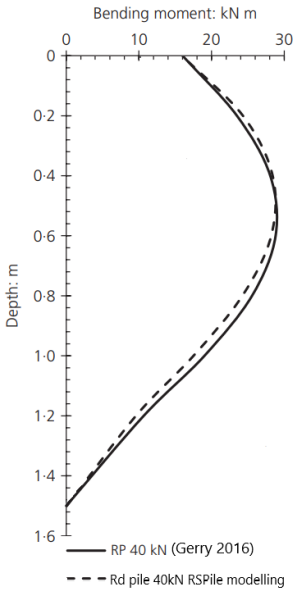

Figure 28. Depth-moment results comparison

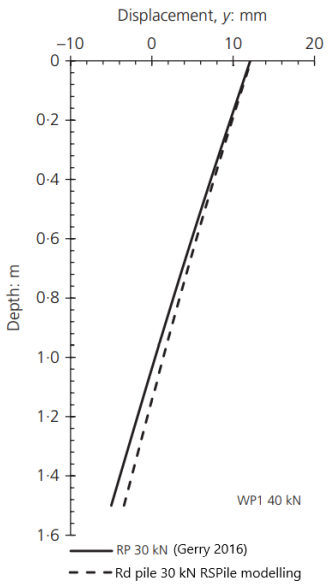

Figure 27. Depth-displacement results comparison

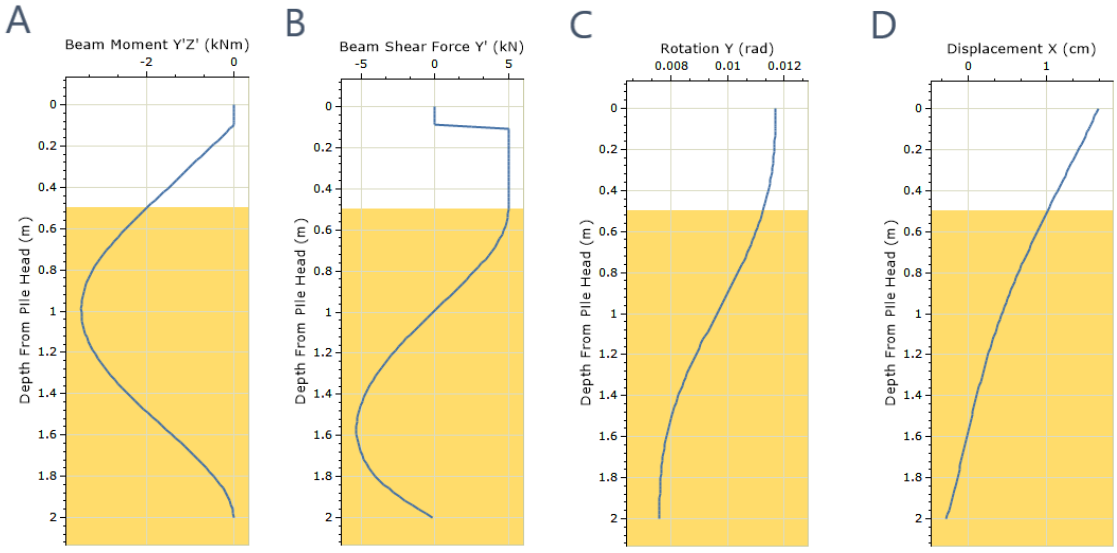

Figure 29. 30 kN laterally loaded RSPile modelling results

A--Bending moment curve B--Shear force curve

C--Rotation curve D--Displacement curve

After confirming that the model can meet the accuracy requirements of numerical simulation, the model experimental data are checked by changing parameters to confirm the accuracy of the model experimental results. By using RSPile, the full model is used for three-dimensional numerical analysis. Pile foundation diameter is divided into D = 19mm, 32mm and 50mm, embedded depth L_{em} = 200mm, 250mm and 300mm, and horizontal load eccentricity e = 335mm. In order to avoid the effect of model boundary on numerical simulation results, the total thickness of foundation soil in the model is 1.5mm, and the distance between pile centre and horizontal boundary is 500mm, which meets the requirements of minimum boundary size.

In the process of numerical simulation analysis, the pile-soil contact surface is set around the pile and at the pile bottom. In case of large difference in material stiffness on both sides of the contact surface, the normal and tangential stiffness of the contact surface can be determined according to the equivalent stiffness of the softer side to ensure the coordination of system deformation.

The subject of this study is the behaviour of monopile under horizontal load, and the behaviour change mainly includes two parts: the change of laterally load and the change of bending moment. Therefore, in order to ensure the accuracy of the experiment, it is necessary to verify the experimental data through RSPile. Due to the repeatability of 12 experiments, test 1, test 4 and test 7 are taken as one of the comparative experiments to verify the effect of different diameters of piles on the horizontal bearing capacity of piles. Another set of comparative tests included test7, test8 and test9. These three tests verify the effect of different buried depth on the horizontal bearing capacity of piles.

After inputting the soil properties and pile properties into RSPile, all kinds of data are obtained by applying the same load. Table 6 shows different modelling tests. The pile type is hollow pipe with the different diameters, embedment depth and different cross section shapes. In Table 6, RD means round pile, SQ means square pile and the RM means the round pile simulation with the real-life size.

Figure 30 shows the same laterally loaded comparison that the experiment data and RSPile simulation with different diameters. Due to the limitation of software, the unloading experiment cannot be carried out, so it presents an open curve. The points in the figure represent the results of the model experiment and the line means the results of the RSPile modelling. In the experiment, the pile is unloaded when the pile reaches

the maximum displacement, so it presents a closed curve shape. In the comparison of results, only the load loading stage is considered. Therefore, although some data do not match, the approximate trend of load displacement curve is similar, which shows that the model experimental results are accurate.

Similarly, Figure 31 shows the horizontal bearing capacity of piles with different embedment depths. The comparison results show that RSPile modelling results are almost consistent with the experimental results, which also shows that the previous experimental results are accurate. In addition, square piles of SQ1, SQ2 and SQ3 are investigated. As can be seen from Figure 32, RSPile is also consistent with the experimental data. Therefore, it can be seen from the comparison results that the model established by RSPile can be used for numerical simulation of pile

Table 6. Modelling tests by RSPile

pile	Embedded length of pile,L (m)	Pile diameter, D (m)	designed L/D	Total length of pile	Pile thickness, t (mm)	Load position, h (m)	h/D	Installed slenderness, L/D
RD1	0.2	0.019	10.5	1.008	1.5	0.473	24.89	10.49
RD2	0.25	0.032	7.8	1.008	1.5	0.423	13.22	7.79
RD3	0.3	0.05	6	1.008	1.5	0.373	7.46	6
RD4	0.2	0.019	10.5	1.008	1.5	0.473	24.89	10.49
RD5	0.25	0.032	7.8	1.008	1.5	0.423	13.22	7.79
RD6	0.3	0.05	6	1.008	1.5	0.373	7.46	6
RD7	0.2	0.019	10.5	1.008	1.5	0.473	24.89	10.49
RD8	0.25	0.032	7.8	1.008	1.5	0.423	13.22	7.79
RD9	0.3	0.05	6	1.008	1.5	0.373	7.46	6
SQ1	0.2	0.05	6	0.855	2.5	0.32	6.4	5.97
SQ2	0.25	0.05	6	0.855	2.5	0.27	5.4	5.97
SQ3	0.3	0.05	6	0.855	2.5	0.22	4.4	5.97
RM1	0.3	0.06	5	1.05	7	0.415	6.92	5
RM2	0.5	0.09	5.6	1.24	7	0.415	4.61	5.57
RM3	1	0.18	5.6	1.86	7	0.415	2.31	5.57
RM4	2	0.35	5.7	3.01	10	0.675	1.93	5.69
RM5	5	0.77	6.5	7.45	10	2.115	2.75	6.5
RM6	10	1.45	6.9	15.75	14	5.415	3.73	6.9

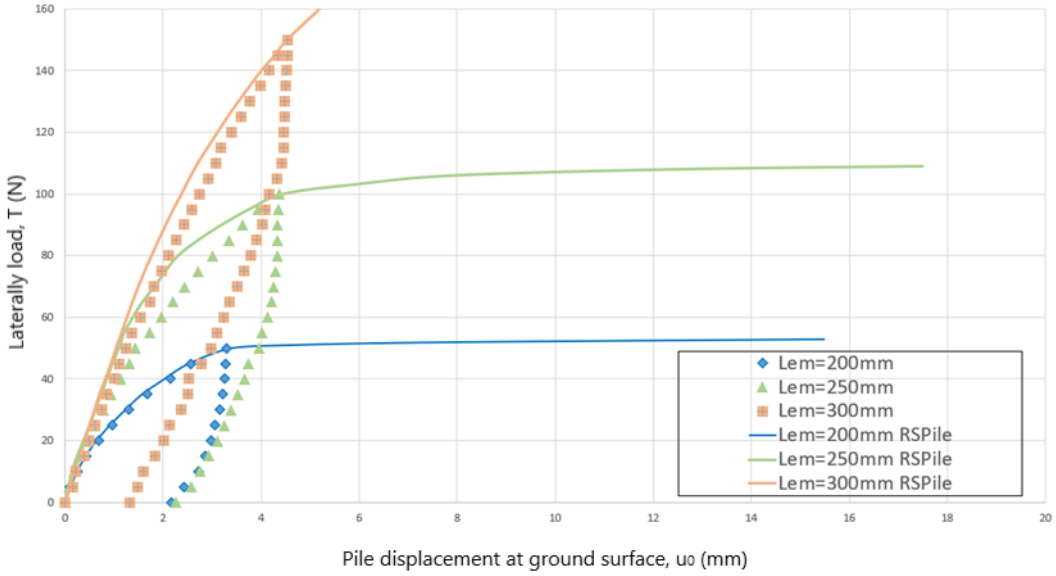

Figure 30. The modelling checking with the different diameter pile.

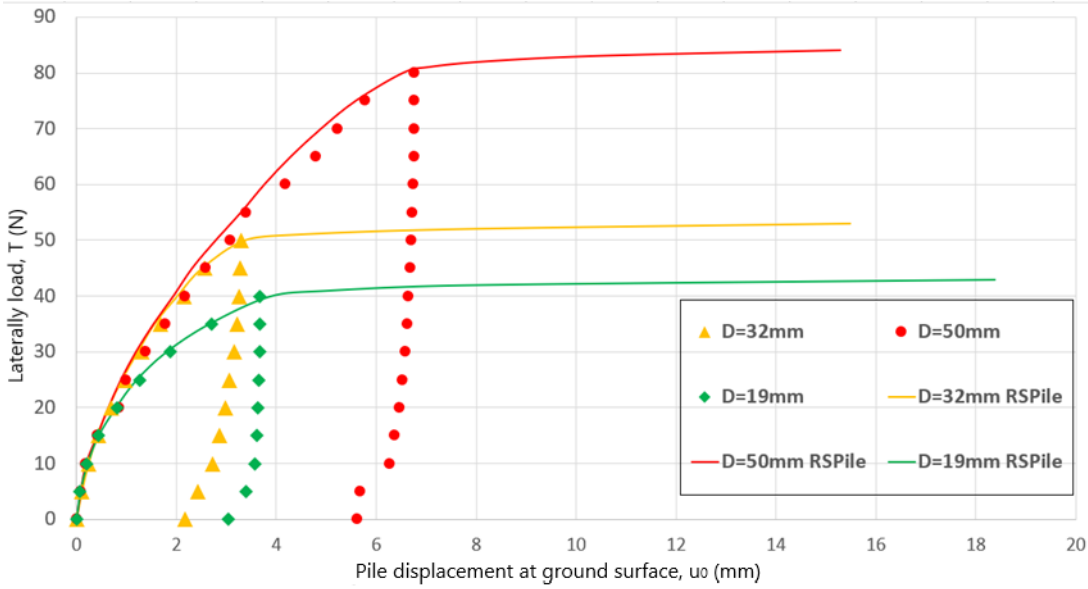

Figure 31. The horizontal bearing capacity of piles with different embedment depths

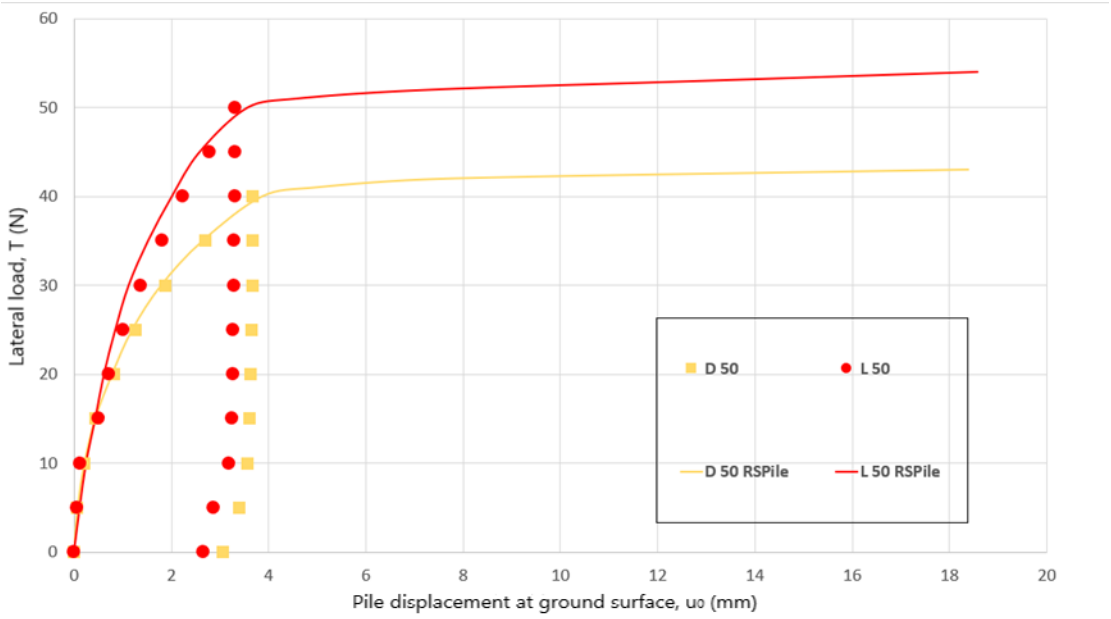

Figure 32. Horizontal bearing capacity of piles with circular section and rectangular section under the same lateral load

In order to verify the relationship between bending moment and depth in model test, the data of model test and numerical simulation are compared in this paper. Figure33 shows the diameter effect on moment-depth curve. It can be found from the picture that the maximum bending moment obtained from the model experiment is slightly greater than that obtained from the numerical simulation. Similarly, the depth of the maximum bending moment in the model experiment is slightly deeper than that in the numerical simulation. However, the bending moment-depth curves of those two results are similar. Therefore, it can be considered that the results of model experiment are consistent with the results of numerical simulation.

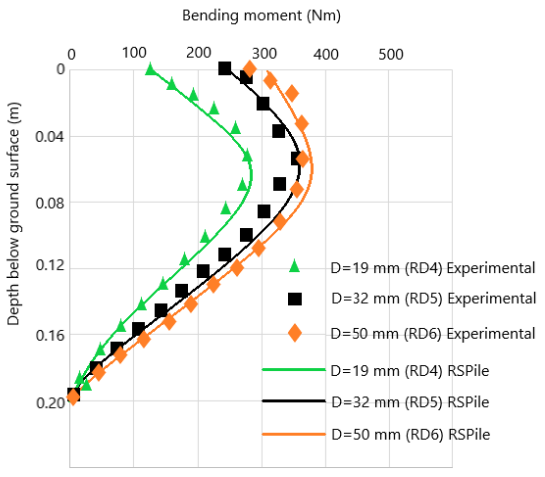

Figure 34. Diameter effects on the bending moment

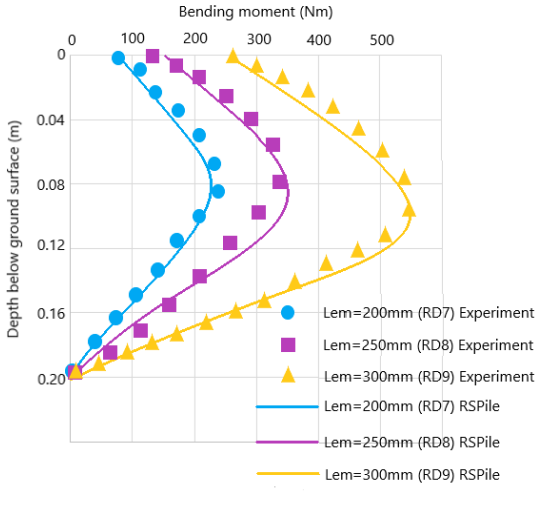

Figure 33. Embedment depth effects on the Bending moment

Figure34 shows the embedment depth effect on moment-depth curve. From the comparison results, it can be found that the maximum bending moment of model experiment is less than that of numerical simulation. However, the depth of the maximum bending moment is basically the same whether in model experiment or numerical simulation. The difference is that when the depth L_{em} of the pile embedded in the soil is 250m and 300mm respectively, there is little difference between the simulation data and the experimental data. However, when L_{em} = 200mm, the maximum bending moment measured by model experiment is far less than that obtained by numerical simulation.

5.2.4. Simulations

After confirming the accuracy of RSPile results in the previous step, the 12 tests were simulated through RSPile. According to the experimental requirements, the basic assumptions need to be set before the simulation of the model:

（1） The pipe pile has been installed, and the installation factors are not considered.
（2） Consider soil consolidation and eliminate the effect of soil consolidation on calculation
（3） Drainage in soil is considered and analysed by total stress method
（4） The soil is a mean elastic-plastic body subject to p-y curve method, and the pile is regarded as a linear elastic material.
（5） Adjusting soil and pile parameters
（6） Apply horizontal load step by step at the fixed position of the pile
（7） According to the RSPile results, the displacements at the soil surface on different pile depth displacement curves are collected
（8） Draw the bending moment displacement curve and load displacement curve for piles with different pile diameters and different buried depths.

The calculated thickness of soil layer = 1.5m, the radial range of the model = 1m, the pile penetration depth is 200mm, 250mm and 300mm respectively, and the pile length is 1008mm. P-y method is adopted for pile-soil contact, and the boundary conditions are: fixed constraint at the bottom and radial displacement constraint at the outside.

The 12 tests were simulated by RSPile with same methods. By applying the same load as the model experiment, the lateral load-displacement curve and moment-depth curve were obtained. Due to the repeatability of numerical simulation, three data are selected for comparative analysis only for piles with different embedded depth and different diameter. Because the RSPile analysis results can only show the horizontal displacement of the pile along the depth direction. Therefore, in order to ensure the accuracy of numerical simulation results and show the horizontal bearing capacity of pile under different lateral loads, multiple points are selected on the p-y curve of numerical analysis.

The solid line in Figure 31 shows the load-displacement curve of the pile under the same lateral load, the same pile diameter but different embedded depth of L_{em}=200mm, 250mm and 300mm respectively. The implementation in Figure 30 shows the load-displacement curve of the pile under the same lateral load, the same buried depth but the different pile diameters with D=19mm, 32mm and 50mm respectively

6. Result and Discussion

6.1. Effect of pile diameter on horizontal bearing capacity of monopile

In this experiment, 19mm, 32mm and 50mm diameter piles are analysed respectively. Other control conditions are 1.5mm behind the pile wall and 200mm, 250mm and 300mm deep into the soil respectively. The following are the experimental results of applying load step by step at 335mm from the soil surface. Figure 18 shows the comparison of results of single piles with different diameters. Due to the replication of the data, other results about the different diameters are shown in the appendix.

According to the Figure 18, it can be seen that:

(1) When the penetration depth of the pile is 200 mm, the displacement of the round pile with a diameter of 19 mm at the soil surface is the largest, reaching 6.8 mm. The round pile with a diameter of 50mm has the smallest displacement at the soil surface, only 3.2mm

(2) When the penetration depth of the pile is 250mm, the displacement of the round pile with diameter of 19mm at the soil surface is the largest, reaching 6.7mm. The

round pile with a diameter of 50mm has the smallest displacement at the soil surface, only 4.3mm.

(3) When the penetration depth of the pile is 300mm, the displacement of the round pile with diameter of 19mm at the soil surface is the largest, reaching 6.9mm. The round pile with a diameter of 50mm has the smallest displacement at the soil surface, only 4.5mm.

Based on the numerical results of Finn (2015), he summarized the numerical analysis results into a linear relationship according to the displacement of piles with different diameters in different soil layers. In this numerical simulation, referring to p-y method, RSPile is used to analyse the experimental data, convert the load-displacement curve and moment-depth curve into logarithmic equation, draw all the data in rectangular coordinate system, and find the linear relationship between load-diameter and moment-diameter, as shown in Figures 35 and 36.

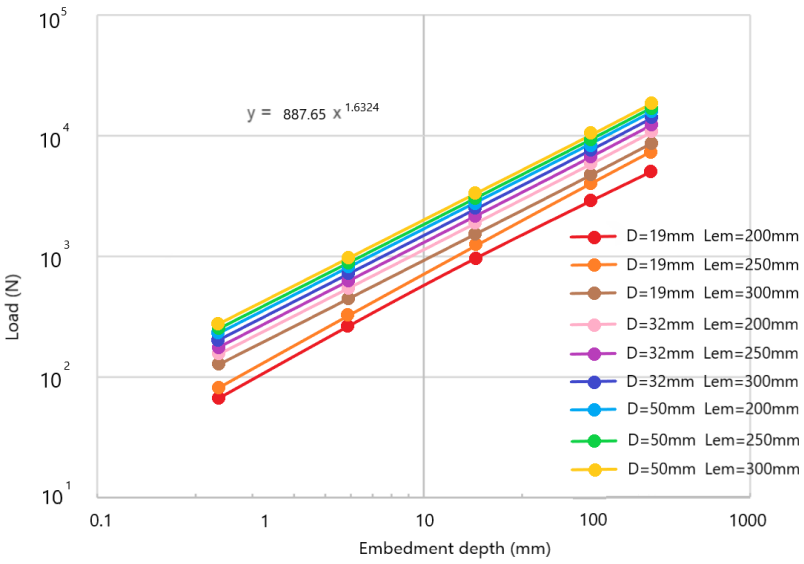

Figure 35. Relationship between laterally load and Embedment depth

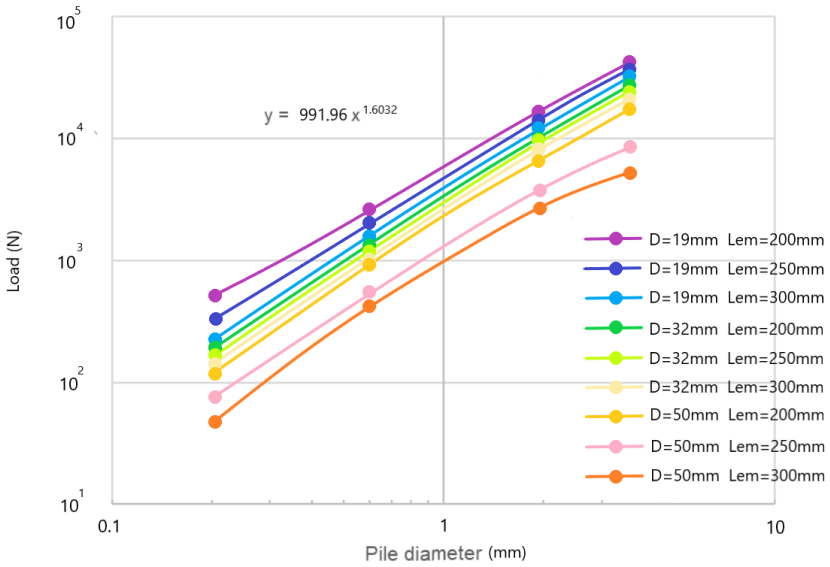

Figure 36. Relationship between laterally load and Pile diameter

In this case study, the piles embedded depth of 200mm, 250mm and 300mm are analysed respectively. Other control conditions are 1.5mm thickness for the model pile, and the cross-sectional diameters of the piles are 19mm, 32mm and 50mm respectively. The following are the experimental results of applying load step by step at 335mm from the soil surface. Due to the repeatability of experiment and numerical simulation. The experimental results are only analysed for Figure 17, and other data are shown in the appendix.

According to the Figure 17, it can be found that:

(1) When the diameter of the pile is 19mm, the displacement of the round pile embedded in the soil depth of 200mm is the largest at the soil surface, up to 4.5mm. The round pile with the depth of 300 mm embedded in the soil has the smallest displacement at the soil surface, only 3.3 mm

(2) When the diameter of the pile is 32mm, the displacement of the round pile embedded in the soil depth of 200mm is the largest at the soil surface, up to 7.1mm. The round pile with the depth of 300 mm embedded in the soil has the smallest displacement at the soil surface, only 6.5 mm.

(3) When the diameter of the pile is 50mm, the displacement of the round pile embedded in the soil depth of 200mm is the largest at the soil surface, up to 5.5mm. The round pile with a depth of 300 mm embedded in the soil has the smallest displacement at the soil surface, only 3.6 mm.

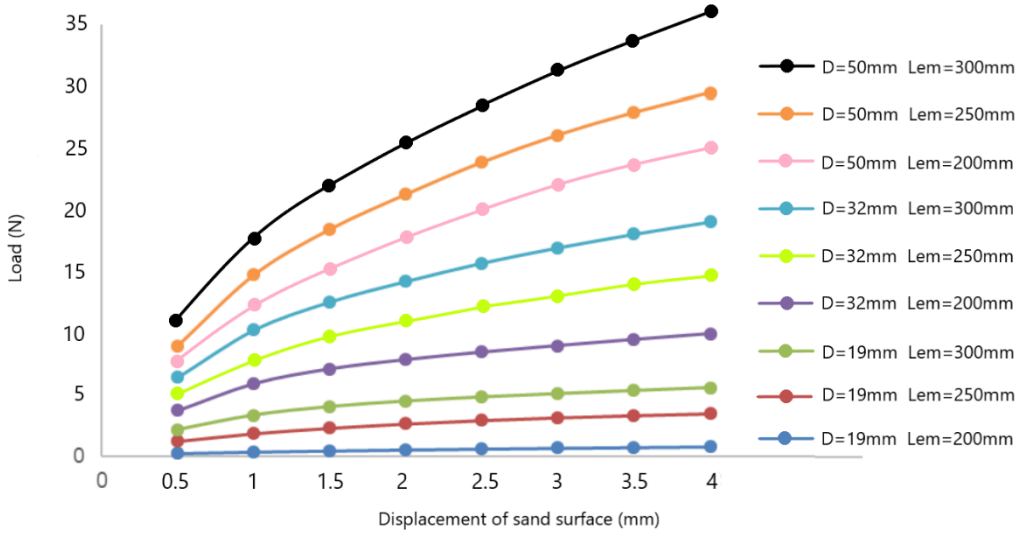

Figure 37. The relationship between laterally load and pile displacement of sand surface

The numerical simulation results of RSPile can only provide the curve of pile displacement varying with depth and the curve of bending moment varying with depth. Therefore, in order to find the relationship between bending moment and pile diameter; For the relationship between the bending moment and the embedment depth of the pile, it is necessary to sort out the data and collect the displacement under different loads at the same position of the pile body. The final sorting result is shown in Figure 37. The other calculation steps are similar to previous steps. The linear relationship is transformed into logarithmic equation. Finally, the relationship between bending moment and pile diameter and between bending moment and pile buried depth is obtained, as shown in Figures 38 and 39.

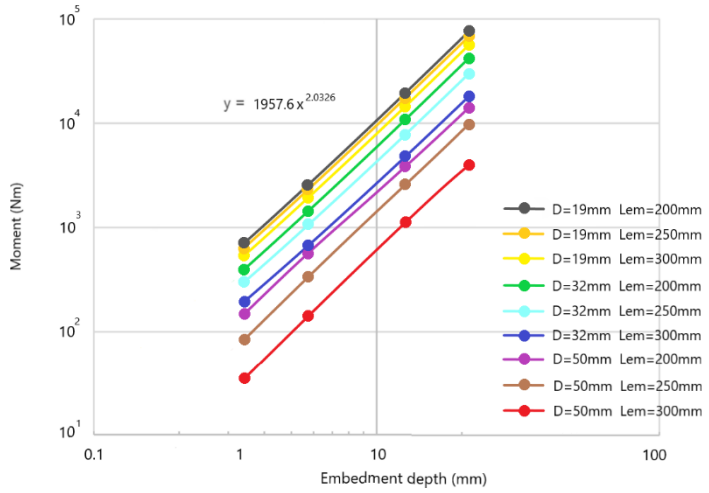

Figure 38. The relationship between bending moment and embedment depth

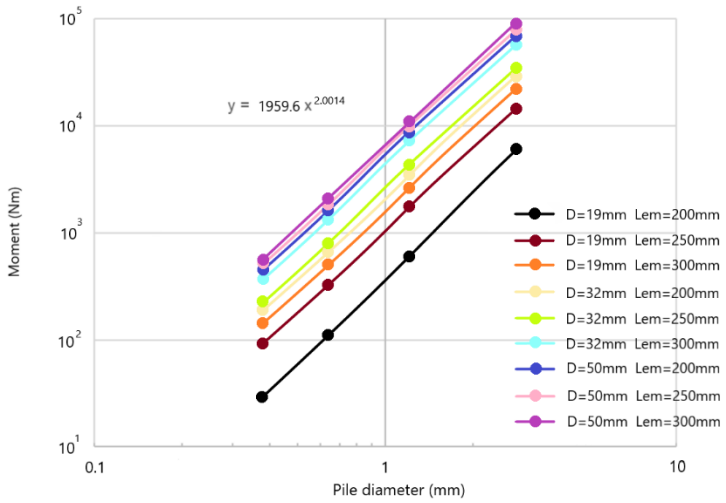

Figure 39. The relationship between bending moment and pile diameter

6.2. Effect of cross section shape on horizontal bearing capacity of monopile

In this experiment, the piles with round and square cross sections are analysed respectively. Other control conditions are 1.5mm thickness, the diameter of the round pile is the same as the side length of the square pile, the same is 50mm, and the embedment depth is 200mm, 250mm and 300mm respectively. The following are the experimental results of applying load step by step at 335mm from the soil surface. Due to the repeatability of experiment and numerical simulation. The experimental results are only analysed for Figure 19, and other data are shown in the appendix.

According to the Figure 19:

(1) When the depth of the pile embedded in the soil is 200 mm, the displacement of the round pile at the soil surface is 4.7 mm. The displacement of square pile at the soil surface at the same depth is 3.3mm.
(2) When the depth of the pile embedded in the soil is 250mm, the displacement of the round pile at the soil surface is 5.1mm. The displacement of square pile at the soil surface at the same depth is 3.1mm.
(3) When the depth of the pile embedded in the soil is 300mm, the displacement of the round pile at the soil surface is 5.6mm. The displacement of square pile at the soil surface at the same depth is 3.9mm.

6.3. Effect of L_{em} / D ratio on monopile

Byme (2015) pointed out that the optimal range of the ratio of pile length to diameter (L_{em}/D) is 3-8 when carrying out the pile model experiment. Two control groups were set in this experiment. The L_{em} / D ratios of tests 1-3 are 10.5, 13.2 and 15.8 respectively, while the L_{em} / D ratios of other tests are in the range of 3-8. Table 6 shows the L_{em} / D ratio of all circular section piles.

The data in Figure 40 shows that the L_{em}/ D of Test 1 is 10.5 and the L_{em} / D of test 2 is 13.2, and their ratios are close to 8. Therefore, there is no special situation in the load unloading stage. The L_{em} / D of test 3 is 15.8, which is far greater than 8. In the load unloading stage of Test3, especially in the initial unloading stage, with the decrease of the force, the displacement of the pile at the soil surface does not change, which is shown as a straight line perpendicular to the Y axis in the force-displacement curve. Then, with the continuous decrease of the load, the force displacement curve becomes a normal curve.

6.4. The change of rotation point

This simulation experiment assumes that the pile will produce displacement on the soil surface, and the pile rotates at the end of the pile. However, through the numerical analysis of the simulation experiment by RSPile, it is found that the pile does not rotate completely with the breakpoint at the bottom of the pile as the centre of the circle.

Figure 40 shows the change of rotation point of the same pile under different horizontal loads。

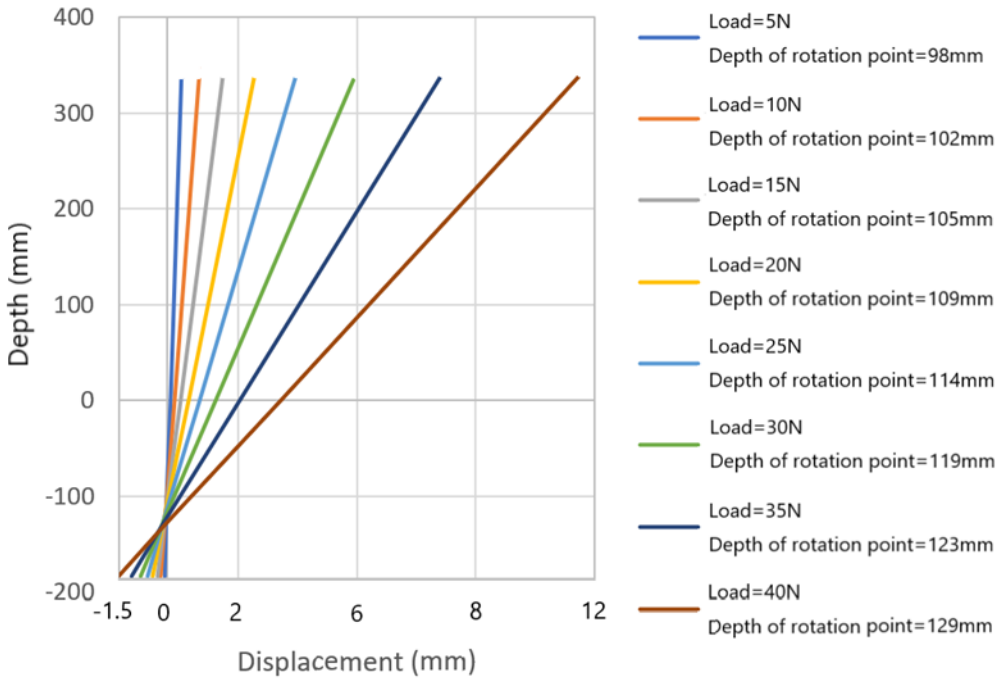

Figure 40. Rotation point moving

12 tests including different diameters, different embedded depths and different cross-sectional shapes were analysed by RSPile. Due to the repeatability of simulation, Figure 40 only shows the change of rotation point of round pile with pile diameter of 19mm and embedded 200 mm in soil. Other data will be shown in Appendix. It can be seen from the data that with the increase of load, the depth from the rotation point to the soil surface gradually deepens. When the horizontal load increases 9 times from 5N to 45N, the depth of rotation point also increases 1.3 times, from 98mm to 129mm.

6.5. Pile displacement simulation

Based on all the above model experiments and the numerical simulation of the model experiment through RSPile, the numerical model based on the study case is obtained. The advantage of numerical simulation is that the pile-soil interaction under actual conditions can be quickly deduced through the set model. The advantage of numerical simulation through RSPile is that it cannot only save the time of field test, but also greatly reduce the cost. Figures 41 and 42 respectively show the displacement of piles

with different pile diameters and different embedded depths under laterally load based on the RSPile model.

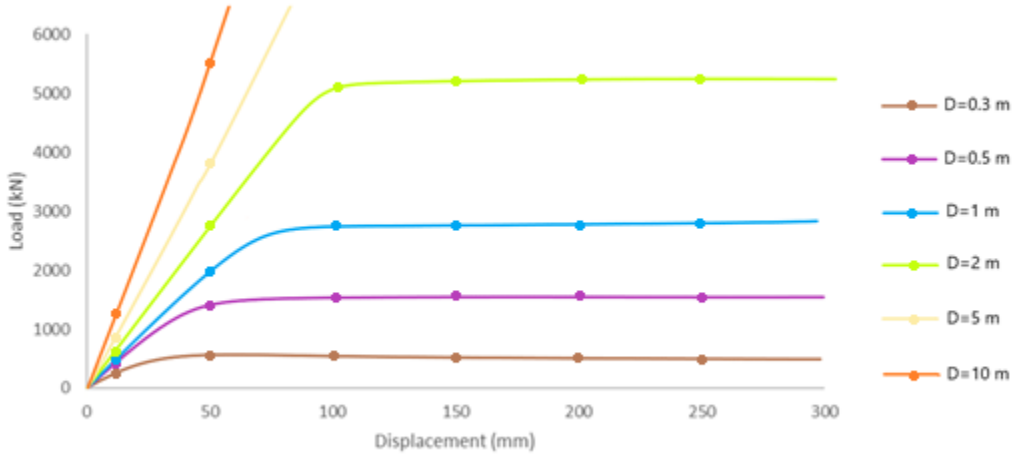

Figure 41. Pile diameter-displacement simulation based on RSPile

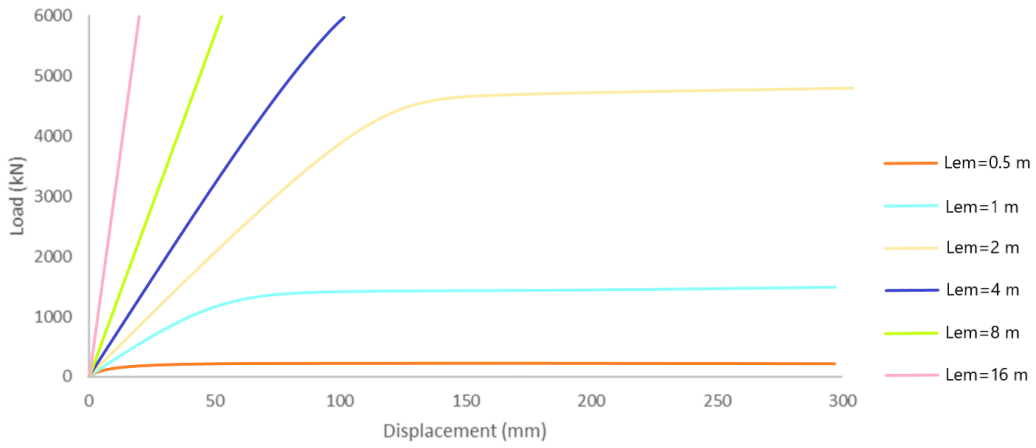

Figure 42. Pile embedment depth-displacement simulation based on RSPile

7. CONCLUSIONS

In this study case, the horizontal bearing characteristics of large diameter monopile are studied by using RSPile numerical simulation software. Based on the research of the bearing capacity of monopile, combined with the field experiment done by Gerry (2016) in the UK, a series of simulation experiments were carried out, and the stability of the pile was studied and checked. According to the results, the specific conclusions are as follows:

（1） The larger diameter of the pile, the smaller displacement of the pile under the same horizontal load. The relationship between the displacement and the diameter can be expressed as:

$$\boldsymbol{Load} \propto \boldsymbol{D^{1.6032}e^{c}} \tag{15}$$

Where D = pile diameter

e^c = the exponent of a constant that depends on displacement level.

In Equation (15), the parameter c, a constant that depends on displacement level, has the following values: 1.47 for 0.005 m displacement; 1.76 for 0.008 m displacement; and 2.05 for 0.011 m displacement.

$$\boldsymbol{Moment} \propto \boldsymbol{D^{2.0014}e^{c}} \tag{16}$$

In Equation (16), the parameter c, a constant that depends on displacement level, has the following values: 2.78 for 0.007 m displacement; 2.89 for 0.009 m displacement; and 3.02 for 0.013 m displacement.

（2） The pile is embedded deeper, the horizontal bearing capacity would be better of monopile. At the soil surface, the relationship between laterally load and embedment depth can be expressed as:

$$\boldsymbol{Load} \propto \boldsymbol{E^{1.6324}e^{c}} \tag{17}$$

In Equation (17), the parameter c, a constant that depends on displacement level, has the following values: 3.16 for 0.015 m displacement; 3.42 for 0.019 m displacement; and 3.97 for 0.026 m displacement.

$$\boldsymbol{Moment} \propto \boldsymbol{E^{2.0326} e^{c}} \quad (18)$$

In Equation (18), the parameter c, a constant that depends on displacement level, has the following values: 3.88 for 0.021 m displacement; 4.17 for 0.026 m displacement; and 4.42 for 0.029 m displacement.

The parameter c of equations (15), (16), (17) and (18) defines the curve to be used for estimating the displacement for a given load or the load to achieve a specified displacement of a pile with a given diameter D. The c for intermediate values of displacement may be obtained by interpolation.

(3) The ratio of pile length to pile section diameter is one of the factors affecting pile deformation. In the model test, when the L_{em}/ D range is between 3-8, the model pile can be regarded as a rigid structure. When the L_{em} / D is far more than 8, the model pile will undergo elastic deformation under horizontal load. Based on the Figure 22, the additional stress on the rigid pile is inversely proportional to the depth and decreases linearly with the increase of depth.

(4) Under the same soil and pile properties, the square pile has a smaller displacement than the same size round pile. The bearing capacity of square pile and the lateral load present a nonlinear relationship, the displacement of square pile at the sand surface is 1.5-1.6 times of the round pile.

(5) When the laterally load acts on the pile, the pile will rotate with the point while generating horizontal displacement, and the rotation point will move downward along the pile with the increase of load. In this model test, after the load is applied, the distance that the rotation point away from soil surface is about 1.3-1.5 times of the load value.

8. FUTURE WORK

The research on the horizontal bearing capacity of large-diameter steel pipe monopile is not mature, which involves the load transfer mechanism and is related to the scale soil conditions of the pile. In this study case, many factors affecting the bearing capacity of large-diameter steel pipe pile are studied, and the pile-soil structure is further studied by numerical simulation with the real data of field experiment as auxiliary data. Through laboratory small-scale model test, the variation laws of bearing mode and bearing capacity of large-diameter steel pipe pile with pile section diameter, embedment depth and pile section shape are found, and compared with numerical simulation to verify the applicability and accuracy of numerical simulation method.

The stability of pile plays an important role in the stability of offshore wind turbine. In the above experiments, only preliminary experiments are carried out on the section shape, diameter, and embedment depth of the pile. The content of the experiment is extensive, and no in-depth study is made on the specific details. In the next work, an in-depth study will be carried out for one part. For example, the displacement and deformation of piles with different cross-section shapes under horizontal load, and the interaction between pile and soil. The field experiment can reflect the real situation of pile-soil interaction. Therefore, the field test is one of the necessary parts for the next study.

From the previous data, it showed that both the diameter and the embedment depth of the pile have the greatest impact on the horizontal bearing capacity of the pile. However, it is limited by the experimental equipment and time. Therefore, it cannot to be further studied. In the following work, sensors will be installed on the body of the model pile for measurement. On the one hand, the relationship between the depth of the pile into the soil and the horizontal bearing capacity of the pile is determined. On the other hand, due to the complexity of the pile-soil action below the surface, the sensor will effectively detect the deformation of the pile under the action of soil reaction.

The stress mode and calculation method of large-diameter pile need to be further studied, and the pile-soil structure needs to be further reasonably optimized, to popularize the research results to practical engineering.

9. REFERENCES

Achmus M, Kuo Y-S, Abdel-Rahman K. Behavior of monopile foundations under cyclic lateral load. Comput Geotech 2009;36:725–35. http://dx.doi.org/10.1016/j. compgeo.2008.12.003.

API. 2007. API RP2A WSD: Recommended practice for planning, designing and constructing fixed offshore platforms – Working stress design, 22nd ed. American Petroleum Institute, Washington, D.C.

Brinkgreve, R. B. J. (2012). PLAXIS 3D Reference Manual. DNV. (2007). DNV-OS-J101: Design of offshore wind turbine structures. Oslo: Det Norske Veritas.

Brown, D. A., Shie, C. F., and Kumar, M. 1989. ‘‘p-y curves for laterally loaded piles derived from three dimensional finite element model.’’ Proc., 2nd Int. Symp., Numerical Models in Geomechanics, Niagra Falls, Canada, Elsevier Applied Sciences, New York, 683– 690.

Burd H, Byrne B, McAdam R, Houlsby G, Martin C, Beuckelaers W, et al. Design aspects for monopile foundations. In: Proceeding 19th ICSMGE, Seoul; 2017.

Byrne, B.W., McAdam, R., Burd, H.J., Houlsby, G.T., Martin, C.M., Gavin, K., Doherty, P., Igoe, D., Zdravković, L., Taborda, D.M.G., Potts, D.M., Jardine, R.J., Sideri, M., Schroeder, F.C., Muir Wood, A., Kallehave, D. and Skov Gretlund, J. 2015. Field testing of large diameter piles under lateral loading for offshore wind applications. Proc 16th European Conference on Soil Mechanics and Geotechnical Engineering (ECSMGE). Edinburgh, UK

Dijkstra J, Broere W, Heeres OM. Numerical simulation of pile installation. Comput Geotech 2011;38:612–22. http://dx.doi.org/10.1016/j.compgeo.2011.04.004.

EWEA, & Corbetta, G. (2015). EWEA: The European offshore wind industry - key trends and statistics 2014, (January 2015).

Fan C, Long J. Assessment of existing methods for predicting soil response of laterally loaded piles in sand. Comput Geotech 2005;32:274–89. http://dx.doi.org/10. 1016/j.compgeo.2005.02.004.

Finn, W.D.L., and Wu, G. 2013. Dynamic Analyses of an Earthfill Dam on Over-Consolidated Silt with Cyclic Strain Softening. In Proceedings of the Keynote

Lecture, 7th International Conference on Case Histories in Geotechnical Engineering, April 29–May 4, Chicago, US.

Gavin K, O'Kelly B, Adekunte A. A field investigation of vertical footing response on sand. Proc ICE – Geotech Eng 2009;162:257–67. http://dx.doi.org/10.1680/geng. 2009.162.5.257.

Grabe, J., Mahutka, K., & Dührkop, J. (2005). Monopileundungen von Offshore-Windenergieanlagen - Zum Ansatz der Bettung. Bautechnik, 82(1), pp. 1–10.

Huang, A. B., Hsueh C.K., O'Neill M.W., Chern S., and Chen, C. (2001). "Effects of construction on laterally loaded pile groups," Journal of Geotechnical Engineering, ASCE, Vol. 127, No. 5, pp. 385-397.

Kulhawy F, Mayne PW. Manual on estimating soil properties for foundation design; 1990.

Lam, I.P.O., and Martin, G. 1986. Seismic Design of Highway Bridge Foundations. Vol. II, Design Procedures and Guidelines. FHWA Report No. FHWA/RD-86/ 102, Federal Highway Administration, U.S. Department of Transportation, Washington, D.C.

Murphy G, Doherty P, Cadogan D, Gavin K. Field experiments on instrumented winged-monopiles. ICE Proc – Geotech Eng Press 2016;169:227–39. http://dx.doi. org/10.1680/jgeen.15.00134.

Reese, L.C., Cox, W.R., and Koop, F.D. 1974. Analysis of Laterally Loaded Piles in Sand. Paper No. OTC 2080. In Proceedings of the 5th Annual Offshore Technology Conference, Houston, Texas. GESA Report No. D-75-9.

Seed, H.B., Wong, R.T., Idriss, I.M., and Tokimatsu, K. 1986. Moduli and Damping Factors for Dynamic Analyses of Cohesionless Soils. Journal of Geotechnical Engineering, ASCE, 112(11): 1016–1032. doi:10.1061/(ASCE)0733-9410(1986)112: 11(1016).

Terzaghi, K. 1955. Evaluation of coefficients of subgrade reaction. Géotechnique, 5(4): 297–326. doi:10.1680/geot.1955.5.4.297.

Walsh, J.M. 2005. Full-Scale Lateral Load Test of a 3×5 Pile Group in Sand. M.Sc. thesis, Department of Civil and Environmental Engineering, Brigham Young University, UT.

W.R. Cox, L.C. Reese, B.R. Grubbs, Field testing of laterally loaded piles in sand, in: Proceeding of the 6th Annual Offshore Technology Conference, vol. 2, Houston, TX, Paper No. OTC 2079, 1974, pp. 459–472.

Wolf, J. P. 1985. Dynamic soil-structure interaction. Prentice-Hall, Englewood Cliffs, N.J., 466.

Xue J, Murphy G, Doherty P, Igoe D, Gavin K. Optimization technique to determine the p-y curves of laterally loaded stiff piles in dense sand. Geotech Test J 2016;39:20140257. http://dx.doi.org/10.1520/GTJ20140257.

Zdravković, L., Taborda, D.M.G., Potts, D.M., Jardine, R.J., Sideri, M., Schroeder, F.C., Byrne, B.W., McAdam, R., Burd, H.J., Houlsby, G.T., Martin, C.M., Gavin, K., Doherty, P., Igoe, D., Muir Wood, A., Kallehave, D. and Skov Gretlund, J. 2015. Numerical modelling of large diameter piles under lateral loading for offshore wind applications. Proc 3rd International Symposium on Frontiers in Offshore Geotechnics (ISFOG 2015). Oslo, Norway.

10. APPENDIX

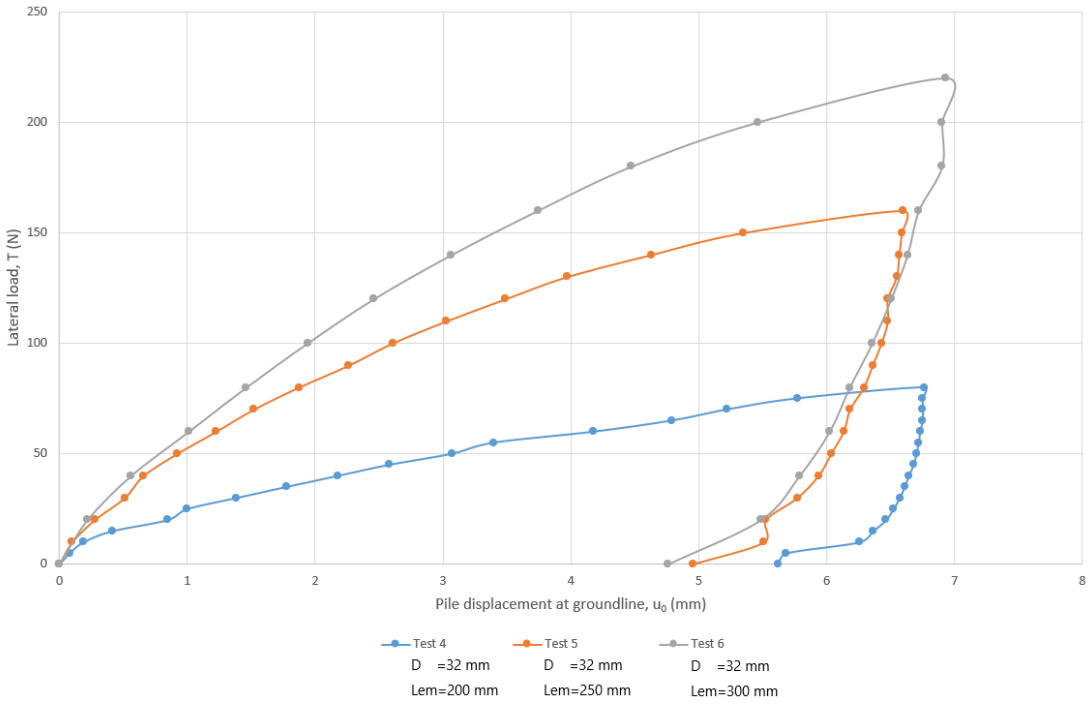

Figure 43. Comparison different embedment depths with 200mm, 250mm and 300mm

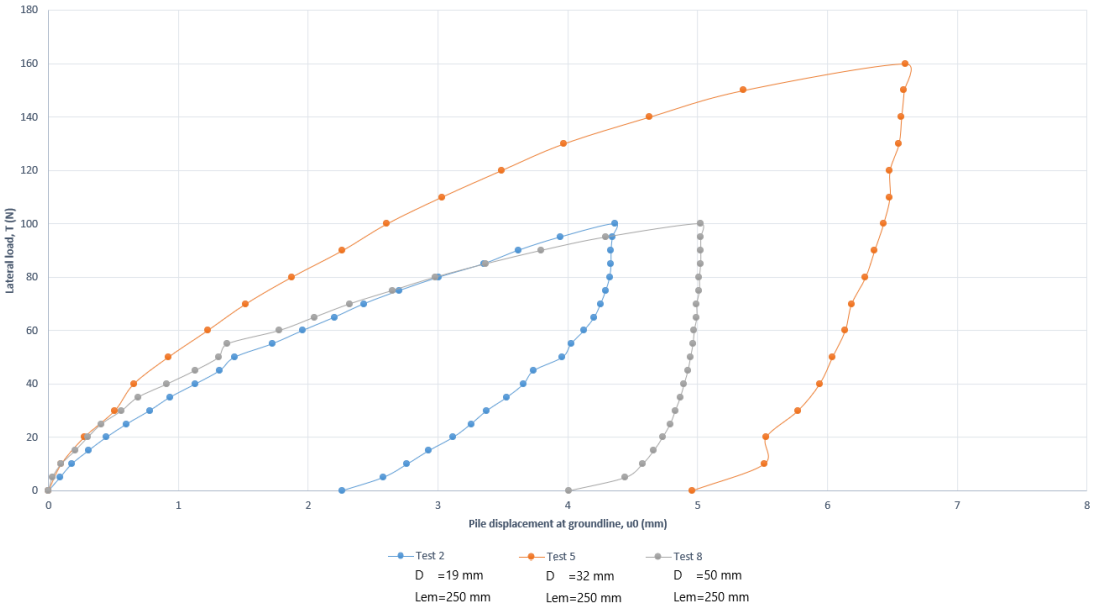

Figure 44. Comparison different diameters with 19mm, 32mm and 50mm

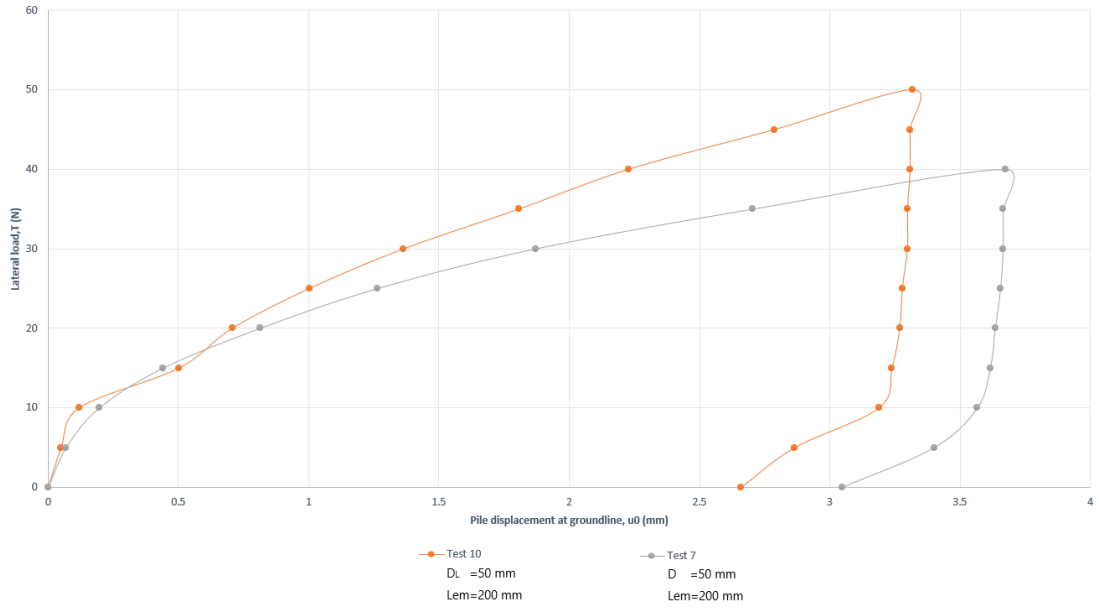

Figure 45. Comparison the displacement with the square pile (test 10) and the round pile (test 7)

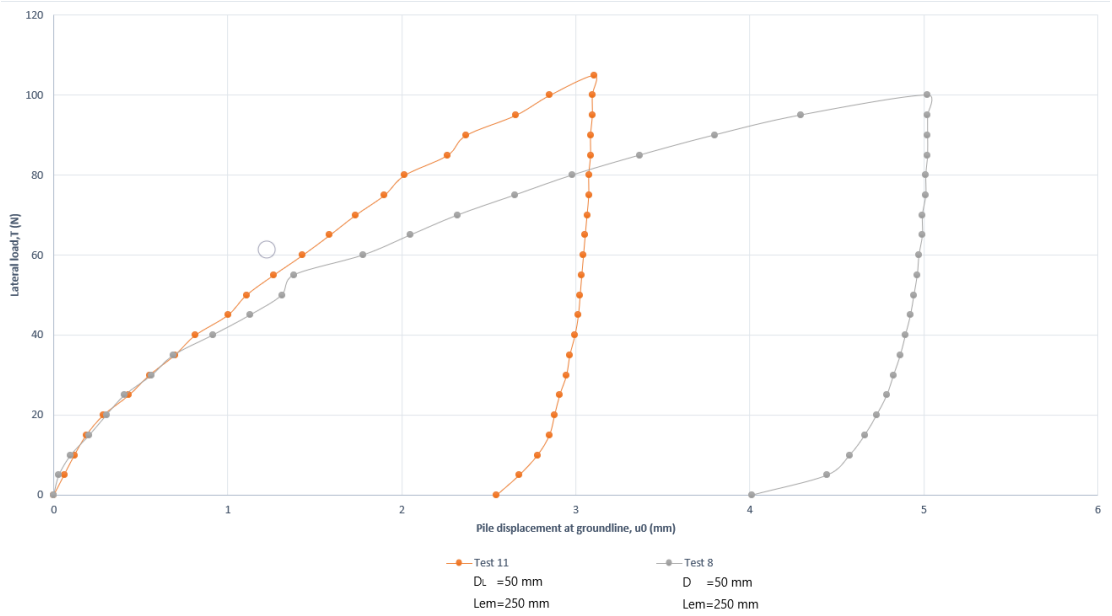

Figure 46. Comparison the displacement with the square pile (test 11) and the round pile (test 8)

A

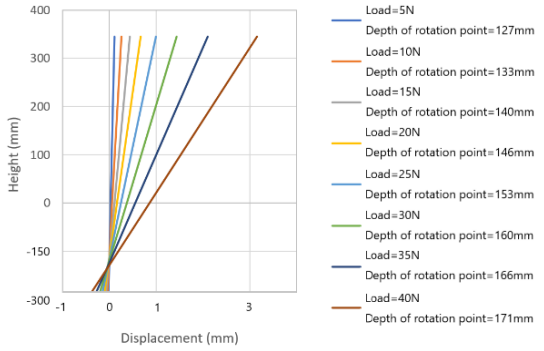
Height (mm)
Displacement (mm)
Load=5N
Depth of rotation point=127mm
Load=10N
Depth of rotation point=133mm
Load=15N
Depth of rotation point=140mm
Load=20N
Depth of rotation point=146mm
Load=25N
Depth of rotation point=153mm
Load=30N
Depth of rotation point=160mm
Load=35N
Depth of rotation point=166mm
Load=40N
Depth of rotation point=171mm

B

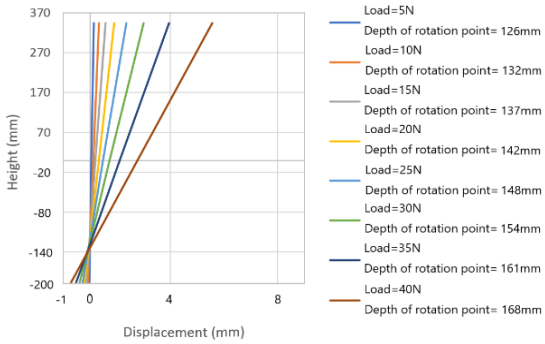
Height (mm)
Displacement (mm)
Load=5N
Depth of rotation point= 126mm
Load=10N
Depth of rotation point= 132mm
Load=15N
Depth of rotation point= 137mm
Load=20N
Depth of rotation point= 142mm
Load=25N
Depth of rotation point= 148mm
Load=30N
Depth of rotation point= 154mm
Load=35N
Depth of rotation point= 161mm
Load=40N
Depth of rotation point= 168mm

C

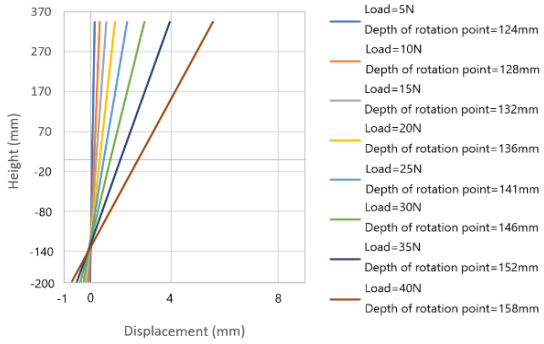
Height (mm)
Displacement (mm)
Load=5N
Depth of rotation point=124mm
Load=10N
Depth of rotation point=128mm
Load=15N
Depth of rotation point=132mm
Load=20N
Depth of rotation point=136mm
Load=25N
Depth of rotation point=141mm
Load=30N
Depth of rotation point=146mm
Load=35N
Depth of rotation point=152mm
Load=40N
Depth of rotation point=158mm

D

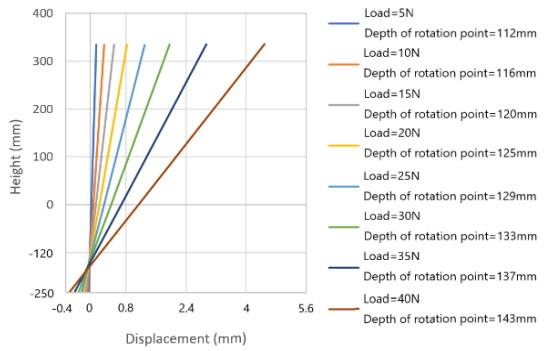
Height (mm)
Displacement (mm)
Load=5N
Depth of rotation point=112mm
Load=10N
Depth of rotation point=116mm
Load=15N
Depth of rotation point=120mm
Load=20N
Depth of rotation point=125mm
Load=25N
Depth of rotation point=129mm
Load=30N
Depth of rotation point=133mm
Load=35N
Depth of rotation point=137mm
Load=40N
Depth of rotation point=143mm

E

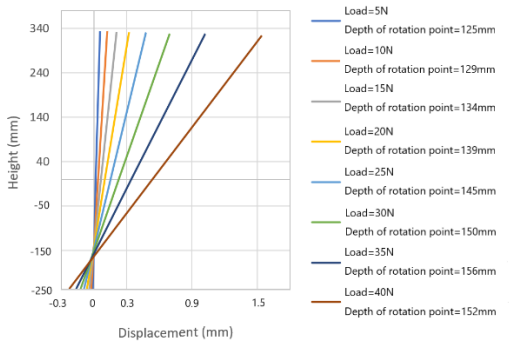
Height (mm)
Displacement (mm)
Load=5N
Depth of rotation point=125mm
Load=10N
Depth of rotation point=129mm
Load=15N
Depth of rotation point=134mm
Load=20N
Depth of rotation point=139mm
Load=25N
Depth of rotation point=145mm
Load=30N
Depth of rotation point=150mm
Load=35N
Depth of rotation point=156mm
Load=40N
Depth of rotation point=152mm

F

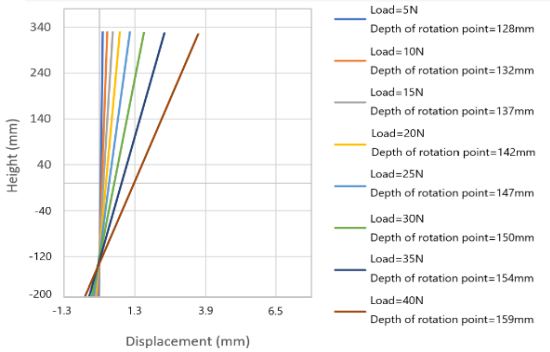
Height (mm)
Displacement (mm)
Load=5N
Depth of rotation point=128mm
Load=10N
Depth of rotation point=132mm
Load=15N
Depth of rotation point=137mm
Load=20N
Depth of rotation point=142mm
Load=25N
Depth of rotation point=147mm
Load=30N
Depth of rotation point=150mm
Load=35N
Depth of rotation point=154mm
Load=40N
Depth of rotation point=159mm

G

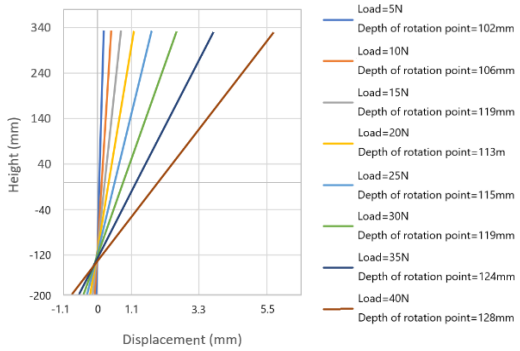
Height (mm)
Displacement (mm)
Load=5N
Depth of rotation point=102mm
Load=10N
Depth of rotation point=106mm
Load=15N
Depth of rotation point=119mm
Load=20N
Depth of rotation point=113m
Load=25N
Depth of rotation point=115mm
Load=30N
Depth of rotation point=119mm
Load=35N
Depth of rotation point=124mm
Load=40N
Depth of rotation point=128mm

H

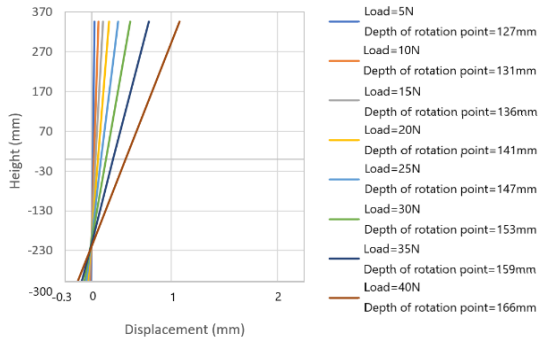
Height (mm)
Displacement (mm)
Load=5N
Depth of rotation point=127mm
Load=10N
Depth of rotation point=131mm
Load=15N
Depth of rotation point=136mm
Load=20N
Depth of rotation point=141mm
Load=25N
Depth of rotation point=147mm
Load=30N
Depth of rotation point=153mm
Load=35N
Depth of rotation point=159mm
Load=40N
Depth of rotation point=166mm

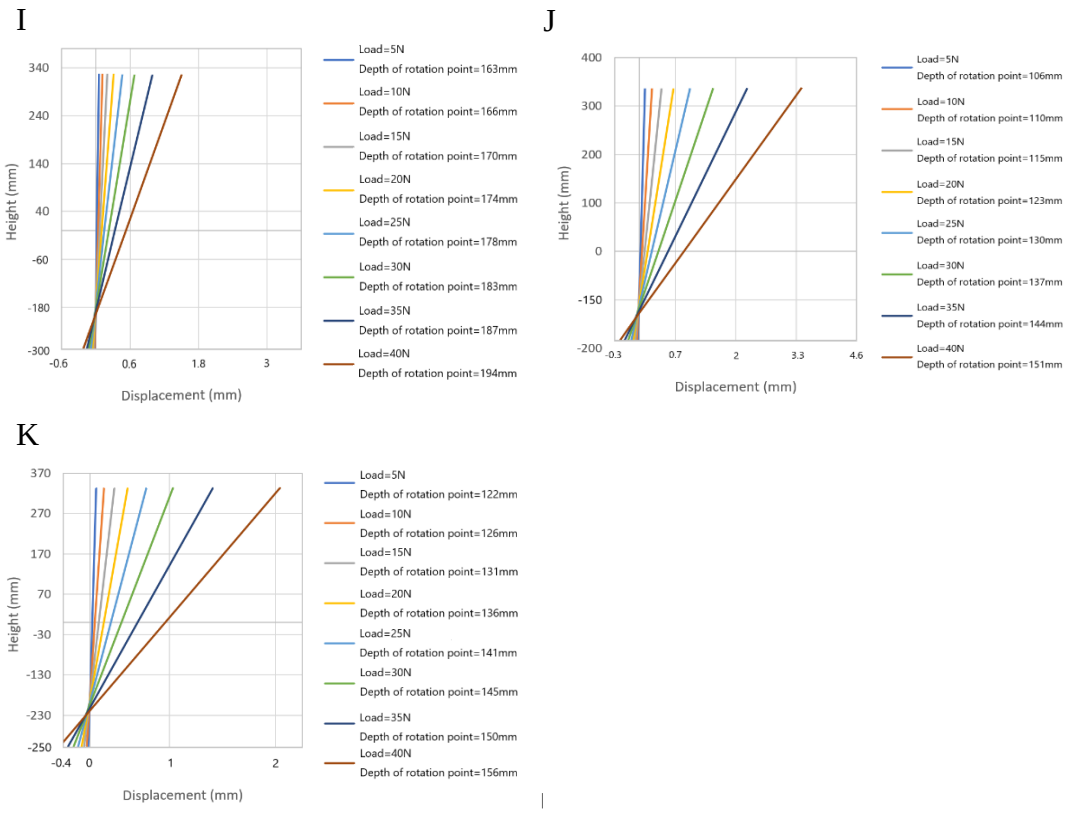

Figure 47. Pile rotation analysis. Diagrams A to K shows the rotation point position under the different laterally load with 5N, 10N, 15N, 20N, 25N, 30N, 35N and 40N.

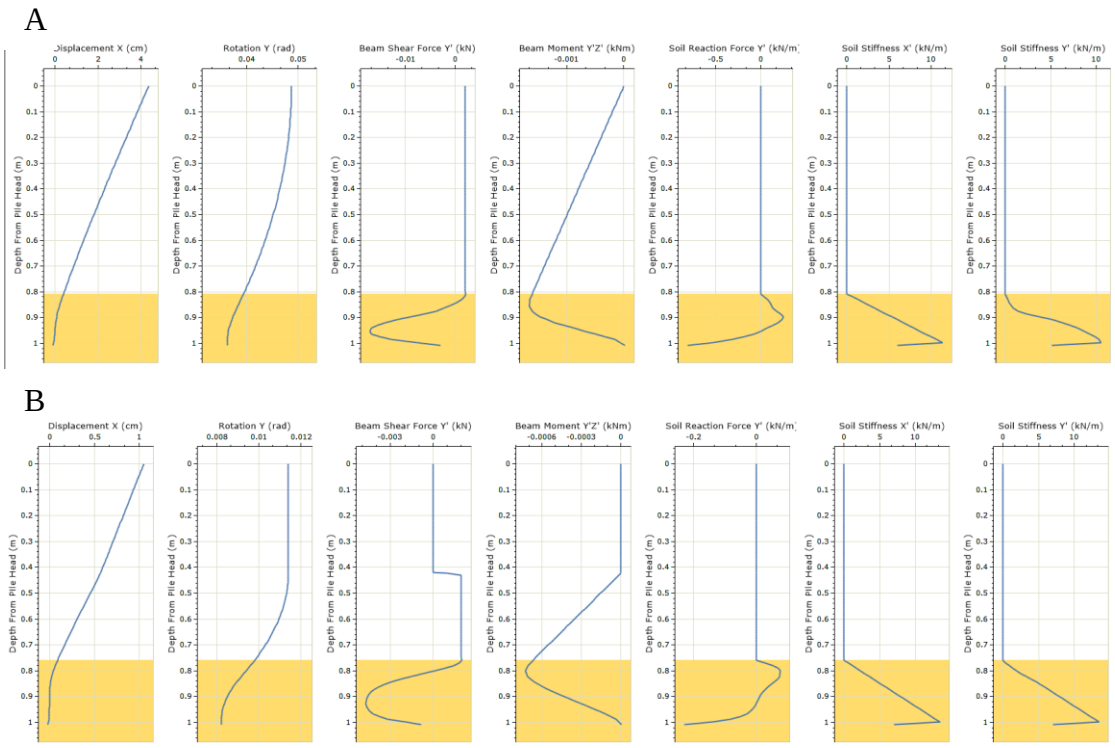

C

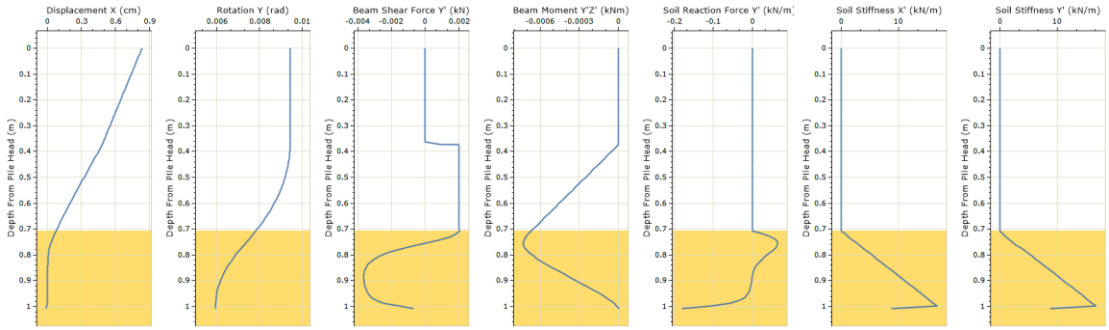
Displacement X (cm)
Rotation Y (rad)
Beam Shear Force Y' (kN)
Beam Moment Y'Z' (kNm)
Soil Reaction Force Y' (kN/m)
Soil Stiffness X' (kN/m)
Soil Stiffness Y' (kN/m)
Depth From Pile Head (m)

D

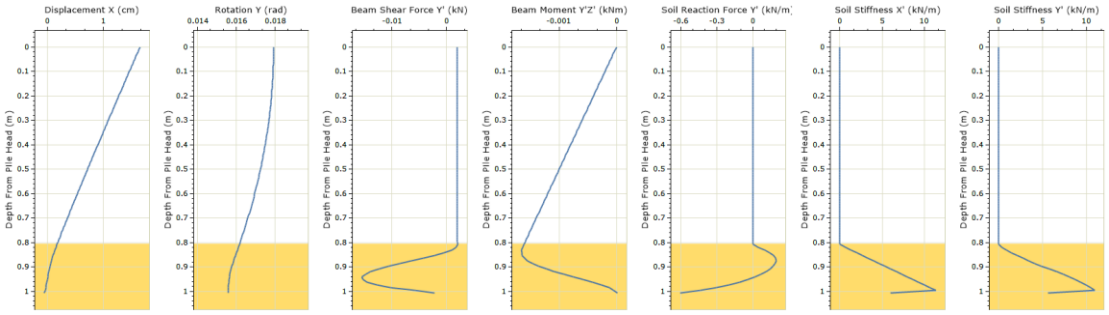
Displacement X (cm)
Rotation Y (rad)
Beam Shear Force Y' (kN)
Beam Moment Y'Z' (kNm)
Soil Reaction Force Y' (kN/m)
Soil Stiffness X' (kN/m)
Soil Stiffness Y' (kN/m)
Depth From Pile Head (m)

E

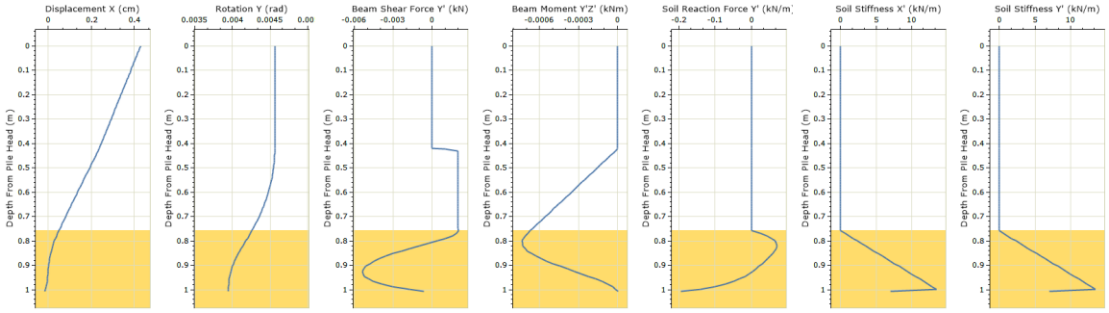
Displacement X (cm)
Rotation Y (rad)
Beam Shear Force Y' (kN)
Beam Moment Y'Z' (kNm)
Soil Reaction Force Y' (kN/m)
Soil Stiffness X' (kN/m)
Soil Stiffness Y' (kN/m)
Depth From Pile Head (m)

F

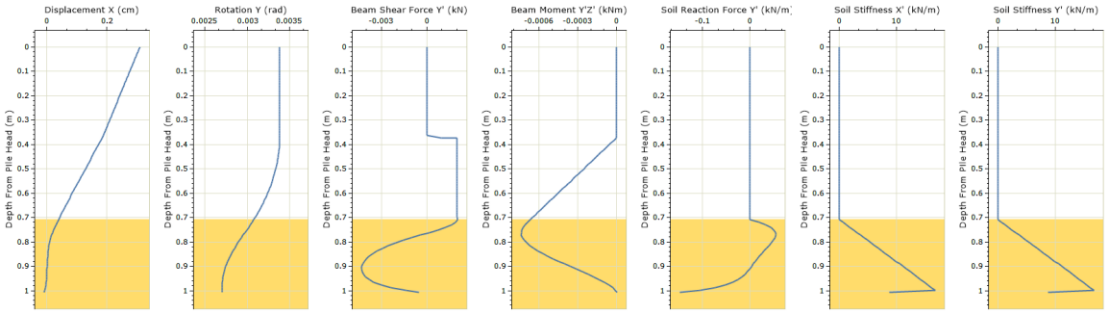
Displacement X (cm)
Rotation Y (rad)
Beam Shear Force Y' (kN)
Beam Moment Y'Z' (kNm)
Soil Reaction Force Y' (kN/m)
Soil Stiffness X' (kN/m)
Soil Stiffness Y' (kN/m)
Depth From Pile Head (m)

G

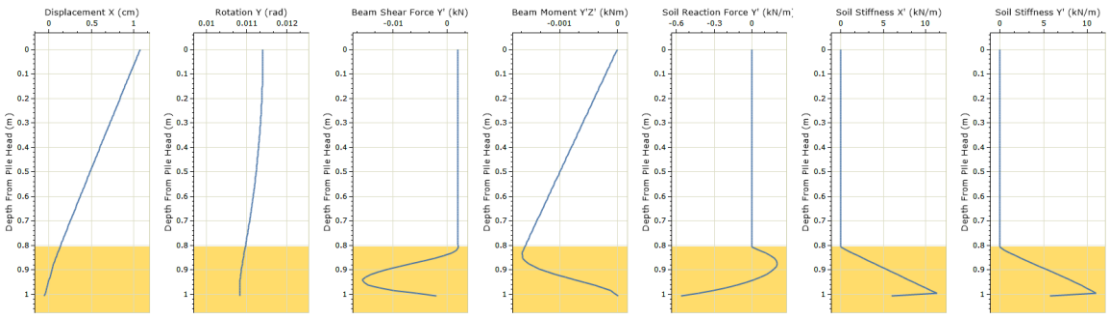
Displacement X (cm)
Rotation Y (rad)
Beam Shear Force Y' (kN)
Beam Moment Y'Z' (kNm)
Soil Reaction Force Y' (kN/m)
Soil Stiffness X' (kN/m)
Soil Stiffness Y' (kN/m)
Depth From Pile Head (m)

H

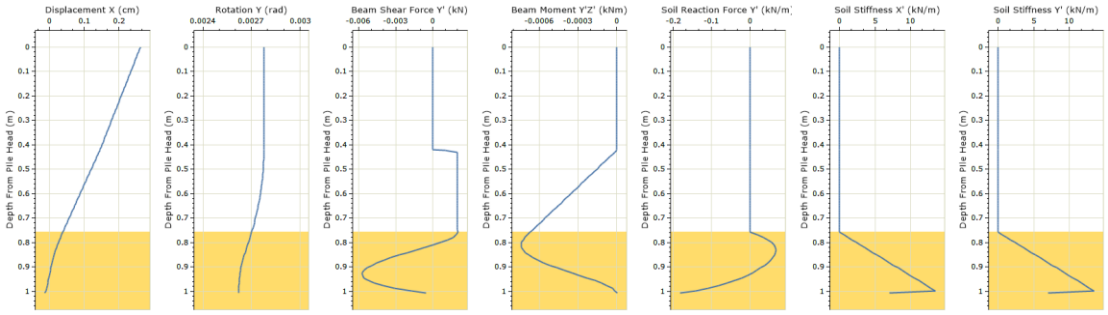
Displacement X (cm)
Rotation Y (rad)
Beam Shear Force Y' (kN)
Beam Moment Y'Z' (kNm)
Soil Reaction Force Y' (kN/m)
Soil Stiffness X' (kN/m)
Soil Stiffness Y' (kN/m)
Depth From Pile Head (m)

I

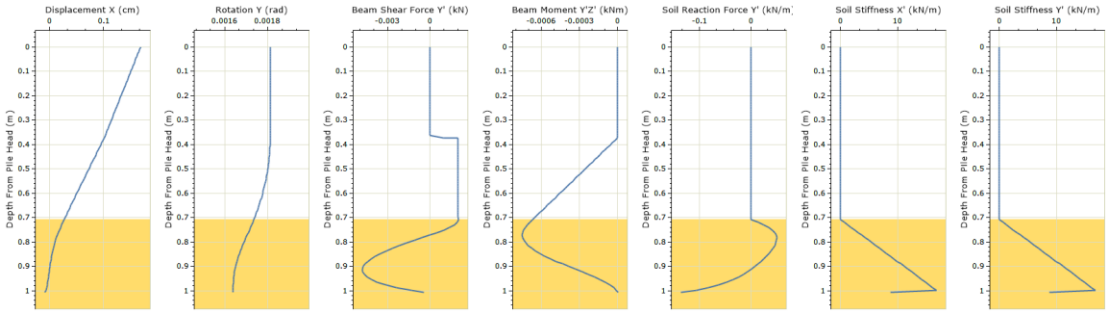
Displacement X (cm)
Rotation Y (rad)
Beam Shear Force Y' (kN)
Beam Moment Y'Z' (kNm)
Soil Reaction Force Y' (kN/m)
Soil Stiffness X' (kN/m)
Soil Stiffness Y' (kN/m)
Depth From Pile Head (m)

J

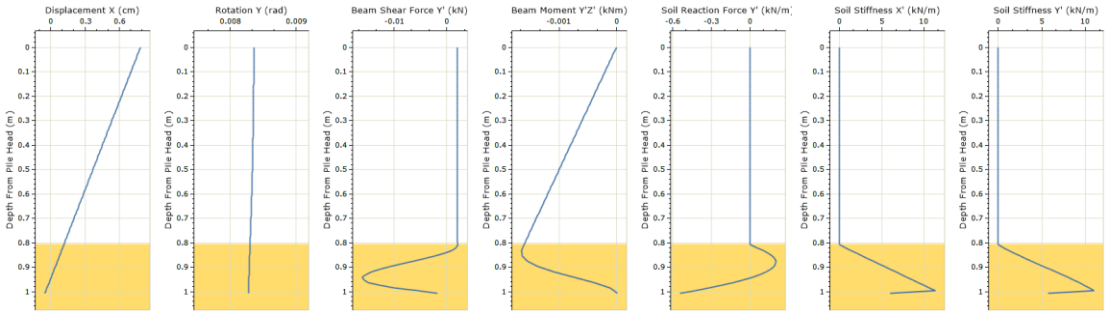
Displacement X (cm)
Rotation Y (rad)
Beam Shear Force Y' (kN)
Beam Moment Y'Z' (kNm)
Soil Reaction Force Y' (kN/m)
Soil Stiffness X' (kN/m)
Soil Stiffness Y' (kN/m)
Depth From Pile Head (m)

K

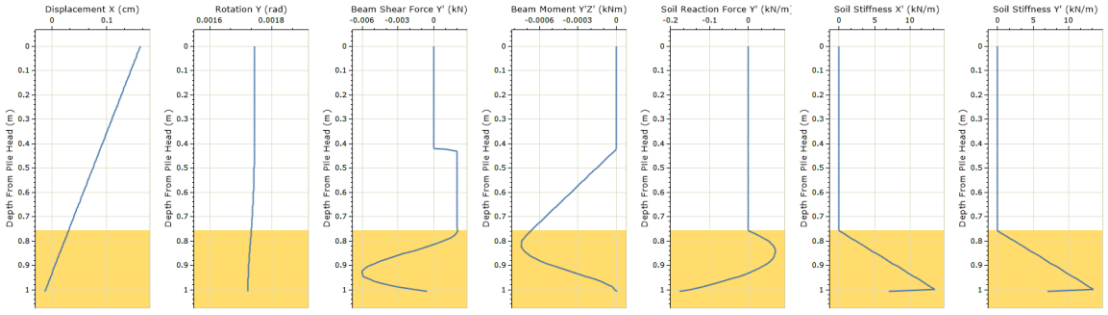
Displacement X (cm)
Rotation Y (rad)
Beam Shear Force Y' (kN)
Beam Moment Y'Z' (kNm)
Soil Reaction Force Y' (kN/m)
Soil Stiffness X' (kN/m)
Soil Stiffness Y' (kN/m)
Depth From Pile Head (m)

L

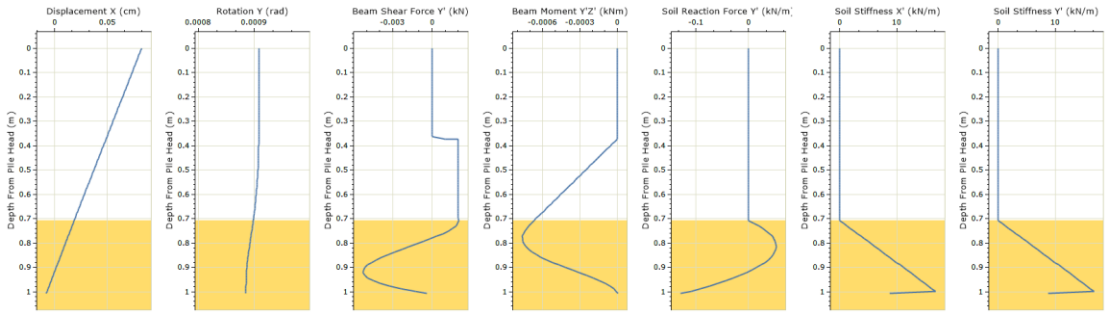
Displacement X (cm)
Rotation Y (rad)
Beam Shear Force Y' (kN)
Beam Moment Y'Z' (kNm)
Soil Reaction Force Y' (kN/m)
Soil Stiffness X' (kN/m)
Soil Stiffness Y' (kN/m)
Depth From Pile Head (m)

Figure 48. RSPile modelling results under 2N laterally load. Diagram A to L present the 12 experiments from test 1 to test 12.

Table 7. Original experimental data for round pile with D=50mm, Lem=300mm (Test9). The green colour shows loading stage and the bule presents unloading phase.

NO.	Weight (kg)	y_R(mm)	y_L(mm)	tanΘ (rad)	p (N)	y (mm)	Θ(rad)	Θ (°)
0	0	0	0	0	0	0	0	0
1	2	0.27	0.18	0.000714286	20	0.177857	0.000714	0.040926
2	4	0.79	0.47	0.002539683	40	0.462381	0.00254	0.145513
3	6	1.3	0.74	0.004444444	60	0.726667	0.004444	0.254646
4	8	1.89	1.06	0.006587302	80	1.040238	0.006587	0.377419
5	10	2.49	1.4	0.008650794	100	1.374048	0.008651	0.495642
6	12	3.17	1.77	0.011111111	120	1.736667	0.011111	0.636594
7	14	3.87	2.16	0.013571429	140	2.119286	0.013571	0.777538
8	16	4.59	2.56	0.016111111	160	2.511667	0.01611	0.923019
9	18	5.48	3.06	0.019206349	180	3.002381	0.019204	1.100307
10	20	6.43	3.58	0.022619048	200	3.512143	0.022615	1.295755
11	22	7.47	4.17	0.026190476	220	4.091429	0.026184	1.500261
12	24	8.71	4.86	0.030555556	240	4.768333	0.030546	1.75016
13	26	10.24	5.72	0.035873016	260	5.612381	0.035858	2.054491
14	24	10.23	5.71	0.035873016	240	5.602381	0.035858	2.054491
15	22	10.22	5.69	0.035952381	220	5.582143	0.035937	2.059033
16	20	10.18	5.66	0.035873016	200	5.552381	0.035858	2.054491
17	18	10.14	5.63	0.035793651	180	5.522619	0.035778	2.04995
18	16	10.05	5.58	0.03547619	160	5.473571	0.035461	2.031784
19	14	9.94	5.51	0.03515873	140	5.404524	0.035144	2.013617
20	12	9.78	5.41	0.03468254	120	5.305952	0.034669	1.986367
21	10	9.61	5.31	0.034126984	100	5.207619	0.034114	1.954574
22	8	9.39	5.17	0.033492063	80	5.069524	0.03348	1.918237
23	6	9.19	5.05	0.032857143	60	4.951429	0.032845	1.881899
24	4	8.87	4.87	0.031746032	40	4.774762	0.031735	1.818303
25	2	8.4	4.59	0.030238095	20	4.499286	0.030229	1.731987
26	0	7.49	4.09	0.026984127	0	4.009048	0.026978	1.545701